

A high relative precision color-magnitude diagram of M67

Eric L. Sandquist^{1*}

¹*San Diego State University, Department of Astronomy, San Diego, CA 92182 USA*

ABSTRACT

We have calibrated and combined an extensive set of *BVI* observations of M67 to produce a color-magnitude diagram of stars measured with high relative precision. We have selected stars that are most likely to be single-star members of the cluster using proper motion, radial velocity, and variability information from the literature, and an examination of the most probable color-magnitude diagram locations of unresolved stellar blends. We have made detailed comparisons of our photometry of the selected stars with theoretical models, and discuss the most notable discrepancies. Observations of M67 turnoff stars are a severe test of algorithms attempting to describe convective cores in the limit of small extent, and we find strong evidence of a “hook” just fainter than the turnoff gap. The stars in M67 support assertions that the degree of convective core overshooting decreases to zero for stars with masses in the range $1.0 < (M/M_{\odot}) \leq 1.5$, but that the degree of overshoot is smaller than currently used in published isochrones. We also verify that all current theoretical models for the lower main sequence (with the exception of Baraffe et al. 1998) are too blue for $M_V \gtrsim 6$ even when the sequences are shifted to match M67 near the M_V of the Sun, probably due to a combination of problems with color- T_{eff} transformations and realistic surface boundary conditions for models. Finally, we identify a subset of cluster members with unusual photometry (candidate red giant binaries, blue straggler stars, and triple systems) deserving of further study.

Key words: stars: evolution – stars: fundamental parameters – stars: distances – open clusters: individual (NGC2682) – convection.

1 INTRODUCTION

Color-magnitude diagrams (CMDs) of stellar clusters have long been used as tests of stellar evolution because of the way they constrain the evolution of the luminosity and surface temperature of individual stars. A number of difficulties have to be overcome to ensure the best quality comparisons with theoretical models, and one of these is obtaining a sufficient number of measurements of stellar fluxes in different filter bands. With small numbers of observations, measurement scatter is often the most important issue since the position of a star in the CMD will not simply be dependent on its mass, chemical composition, and evolutionary state. In a cluster of stars, the ensemble of measured stars must then be used to infer where a single star would fall in the diagram. However, with a large enough number of independent observations of a group of stars, the photometric scatter can be reduced to the point where it is no longer a significant contributor to uncertainty in the position of the cluster’s fiducial line. At that point, scatter introduced by

unresolved binaries, variable stars, and nonmembers become the main contributors to the scatter.

With a high-precision photometric database, calibration to a standard system can require relatively little additional effort: a few nights of observations under photometric conditions with fairly large numbers of cluster star observations interspersed with standard star observations covering the color range of the cluster stars to be calibrated and covering the airmass range of the cluster observations. Of course, the standard calibration can also be improved with additional data as long as the standard system is well determined.

There are numerous benefits to high precision CMD studies. First, the shapes of the fiducial lines often reveal inadequacies in our understanding of the stellar physics involved in modeling the stars. An example is the turnoff region of open clusters, where observations have shown that a small amount of convective overshooting in the convective cores of stars is necessary to explain the morphology of the fiducial line. High precision measurements can also reveal the presence of peculiar stars. Two examples are the poorly understood “sub-subgiant branch” stars S1063 and S1113 in M67 (Mathieu et al. 2003; identifications starting with “S” are from Sanders 1977). Both stars are high-probability

* E-mail: erics@mintaka.sdsu.edu

cluster members, but fall in a region of the CMD where it is very difficult to explain their photometric properties.

High-precision photometry can also open up the possibility of spectroscopic studies of the surface properties and abundances by identifying samples of probable single stars. While proper motion studies can identify cluster members, eliminating unresolved binaries from the sample generally requires large investments of time for radial velocity studies. Even so, wide binaries and binaries with extreme mass ratios are unlikely to be identified except with the help of precise photometry. Field star contamination of cluster CMDs can often make the selection of cluster members difficult if proper motion studies have not been carried out. Even when they have been, the first epoch observations were most frequently taken using photographic techniques, which most often means that faint main sequence stars are unlikely to have been included.

These issues are particularly pressing in the case of open clusters like M67. M67 is probably the most thoroughly studied old open cluster in the Galaxy, thanks to its small distance from us. Typically quoted values for the cluster's age (4 ± 0.5 Gyr; Dinescu et al. 1995) place it between the majority of known open clusters and the much older globular clusters. There have also been a number of proper motion membership studies of the cluster (Sanders 1977; Girard et al. 1989; Zhao et al. 1993) and radial velocity studies (Mathieu et al. 1986, 1990) that can be used to help “clean” the CMD of nonmembers and binary stars in order to make the single-star sequence more apparent. A number of authors have commented on the seemingly large binary star fraction in the cluster (Montgomery et al. 1993; Fan et al. 1996), which probably indicates a high degree of mass segregation and may also indicate that the cluster is in the late stages of its dynamical life during which it is being tidally disrupted.

Recent attention on clusters has come from variability studies, and in some cases a by-product of such a study can be a large number of observations of non-varying stars. The dataset we describe below is a result of studies of two particularly difficult eclipsing variables in M67: the blue straggler S1082 ($P = 1.0677978$ d for the eclipsing binary), and the totally-eclipsing variable S986 ($P = 10.33813$ d). We gathered thousands of frames of observations of M67 in V band, hundreds of observations in I , and tens in B . We will focus our attention on the VI CMD because of its high precision. Fan et al. (1996) has also presented wide-field photometry of M67 in nine filters. Their photometry in at least three of those filters (with bandpasses centered at 3890, 6075, and 9190 Å) certainly qualifies as high precision. However, because their photometry was taken in a non-standard filter system, the comparison of their data with theoretical values is more complicated than ours. However, we will use their data in conjunction with ours to attempt to identify the stars that have the highest probability of being single stars.

We briefly describe our photometry and its reduction and calibration in §2. In §3, we present our identification of the single star sequence and determination of the fiducial line. In §4, we compare the fiducial line with theoretical isochrones.

Table 1. Observing Log for Photometry at Mt. Laguna

#	Date	Filters	mJD Start	N_{obs}
1	Jan. 27/28, 2000	BVI	1571.739	22,20,23
2	Dec. 5/6, 2000	V	1884.878	60
3	Dec. 6/7, 2000	I	1885.871	38
4	Dec. 7/8, 2000	V	1886.806	111
5	Dec. 11/12, 2000	V	1890.817	57
6	Dec. 12/13, 2000	V	1891.820	116
7	Dec. 13/14, 2000	B	1892.815	28
8	Jan. 23/24, 2001	V	1933.675	206
9	Jan. 25/26, 2001	V	1935.673	176
10	Jan. 29/30, 2001	V	1939.676	44
11	Jan. 30/31, 2001	V	1940.657	130
12	Jan. 31/Feb. 1, 2001	V	1941.663	161
13	Feb. 17/18, 2001	V	1958.655	63
14	Feb. 18/19, 2001	V	1959.790	75
15	Nov. 14/15, 2001	V	2228.901	74
16	Jan. 20/21, 2002	V	2295.735	91
17	Jan. 21/22, 2002	V	2296.687	89
18	Jan. 24/25, 2002	V	2299.690	124
19	Feb. 5/6, 2002	V	2311.649	119
20	Feb. 10/11, 2002	V	2316.638	167
21	Mar. 18/19, 2002	BV	2352.625	12,131
22	Apr. 13/14, 2002	V	2378.638	103
23	Apr. 18/19, 2002	V	2383.661	47
24	Nov. 21/22, 2002	VI	2600.845	108,25
25	Jan. 17/18, 2003	I	2657.718	192
26	Jan. 22/23, 2003	I	2662.702	110
27	Feb. 17/18, 2003	I	2688.617	147
28	Mar. 20/21, 2003	I	2719.635	138
29	Apr. 20/21, 2003	I	2750.638	150

Note: mJD = HJD - 2450000

2 PHOTOMETRIC OBSERVATIONS AND REDUCTIONS

All of the photometry for this study was taken at the 1 m telescope at the Mt. Laguna Observatory using a 2048×2048 CCD on nights between December 2000 and April 2003. The nights of observations are given in Table 1. Typical exposure times ranged between 10 and 60 s to optimize the counts for our eclipsing binary targets near the cluster turnoff.

Most of the details of the reduction are presented in other papers (Sandquist et al. 2003a, Sandquist & Shetrone 2003b), so we only briefly describe the reduction here. The object frames were reduced in usual fashion, using overscan subtraction, bias frames, and flat fields. We conducted aperture photometry using the IRAF¹ tasks DAOFIND and PHOT from the APPHOT package. In order to improve the accuracy of the relative photometry for the light curves, we used an ensemble photometry method similar to that described by Honeycutt (1992), iterating toward a consistent solution for photometric zeropoints for all frames and median magnitudes for all stars. One major difference with other ensemble photometry techniques involved the use of position-dependent corrections to stellar magnitudes to account for variations in the point-spread function across the

¹ IRAF (Image Reduction and Analysis Facility) is distributed by the National Optical Astronomy Observatories, which are operated by the Association of Universities for Research in Astronomy, Inc., under contract with the National Science Foundation.

frame and for changes in frame centre. Because frames typically had more than 300 measurable stars, the formal errors in the zero points ranged from around 0.003 to 0.007 mag, even with respect to night-to-night variations. Because of the often large number of observations of individual stars, typical errors in star magnitudes were a few millimag to a fraction of a millimag. (Because we relied on robust median magnitudes, these errors were derived in the following way. We first created a list of individual observations of a given star in a given bandpass and found the median. We then took the square-root of the number of observations of the star in the bandpass, and looked up the observations of the star that number of entries away from the median entry in the list ordered by magnitude. The error was taken to be one half of the difference between those observations.)

2.1 Photometric Calibration

We have completed a calibration of our photometric dataset to attempt to ensure accurate placement of our photometry on the standard system. The large numbers of measurements in our studies of M67 has meant that the main sequence scatter is smaller than in either Montgomery et al. (1993) or the more recent Richer et al. (1998), which both used standard Johnson-Cousins filters. Our calibration was taken from a night of photometric data taken at Mount Laguna Observatory on January 27/28, 2000. Observations of the Landolt standard fields SA 95, 97, 98, 101, and 107 were interspersed with observations of M67 through the B , V , and I filters (at least 20 images in each band). We used Stetson (2000) standard values for stars when available, and Landolt (1992) values for the remainder of the standards.

Aperture photometry was performed on both standard and cluster frames using DAOPHOT II (Stetson 1987) using multiple synthetic apertures. Growth curves were used to extrapolate measurements to a (large) common aperture size using the program DAOGROW (Stetson 1990). The photometric transformation equations used in the calibration were

$$b = B + a_0 + a_1(B - V) + a_2(X - 1.25)$$

$$v = V + b_0 + b_1(V - I) + b_2(X - 1.25)$$

$$i = I + c_0 + c_1(V - I) + c_2(X - 1.25) + c_3(V - I)^2 + c_4(V - I)^3$$

where b , v , and i are the observed aperture photometry magnitudes, B , V , and I are the standard system magnitudes, and X is airmass. The transformation coefficients were determined using the program CCDSTD (e.g. Stetson 1992), and with the exception of the I -band data, the data were well fitted by linear color terms.

We selected 197 stars in the central part of the cluster to be our secondary standards. These stars were generally on the lower RGB, subgiant branch, upper MS, or blue stragglers, and covered most of the range of colors for the cluster stars observed ($0 \lesssim (V - I) \lesssim 1.5$). We noticed that the secondary standard observations, once corrected to the standard system, had significant trends with airmass. Since the M67 stars were observed over a wider range of airmasses than the primary standards, we used these trends to derive corrected airmass terms for the transformation equations.

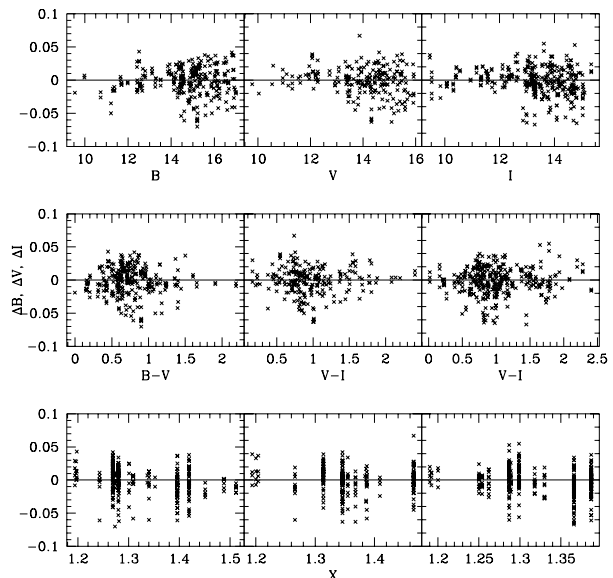


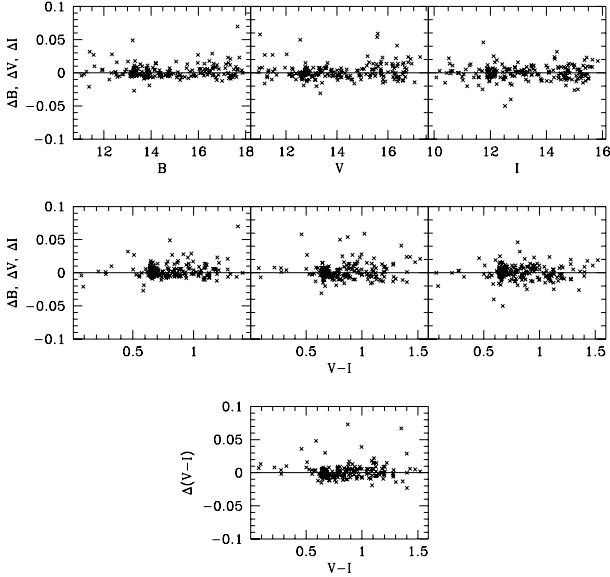
Figure 1. Residuals (in the sense of our observed values minus the standard values) from the calibration of primary photometric standards versus magnitude (top row), color (middle row), and airmass X (bottom row). The first column is for B measurements, the second for V , and the third for I .

The corrected values removed the airmass trends, and did not noticeably affect the quality of the fits to the primary standards, so we adopted the corrected airmass terms for the transformations. The residual plots for the primary standard fits are shown in Fig. 1, and the transformation coefficients are given in Table 2. The calibrated secondary standard values were then used to calibrate our ensemble photometry. We present the transformation coefficients in Table 2. Because physically different filters were used on the night of calibration and during the ensemble photometry, there are significant color terms and there is a significant second-order term present in the I -band residuals. The results of the calibration are shown in Fig. 2. We must emphasize that we can only be confident of the calibration within the range of colors of our secondary standards, and that this is *not* the entire range of colors covered by our ensemble photometry, so that there may be systematic errors in the absolute calibration of the lower main sequence. For the purposes of the distance modulus determination, our photometry appears to be accurately calibrated to the standard system.

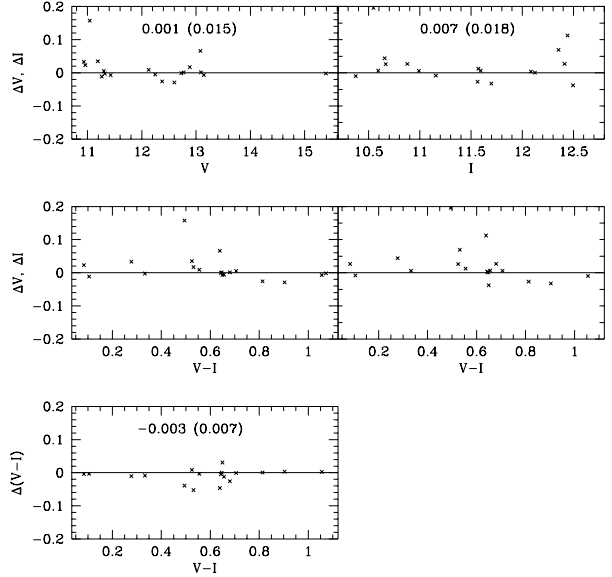
We made comparisons between our dataset and those of Joner & Taylor (1990) and Chevalier & Ilovaisky (1991) (both studies made detailed attempts to tie their photometry to the Landolt standard system), and to Montgomery et al. (1993), which is the most frequently cited source of M67 photometry. We find good agreement between our photometry and values from Joner & Taylor (1990) and Chevalier & Ilovaisky (1991) as shown in Figs. 3 and 4. One exception is the slight zero-point difference in I between our photometry and that of Chevalier & Ilovaisky (1991). We find more substantial differences between our photometry and that of Montgomery et al. (1993), however. In the color range covered by the photometry of Joner & Taylor (1990)

Table 2. Photometric Transformation Equation Coefficients

Filter	Airmass Term		Color Term	
		<u>Primary Calibration</u>		
<i>B</i>	Uncorrected	0.1326 ± 0.0120	First Order	-0.0708 ± 0.0027
	Corrected	0.2168 ± 0.0121	Corrected	-0.0683 ± 0.0030
<i>V</i>	Uncorrected	0.0808 ± 0.0154	First Order	0.0067 ± 0.0027
	Corrected	0.1103 ± 0.0156	Corrected	0.0072 ± 0.0026
<i>I</i>	Uncorrected	0.	First Order	0.0623 ± 0.0150
			Second Order	-0.0888 ± 0.0148
			Third Order	0.0214 ± 0.0043
	Corrected	0.0505 ± 0.0013	First Order	0.0779 ± 0.0156
			Second Order	-0.1020 ± 0.0153
			Third Order	0.0244 ± 0.0045
	<u>Secondary Calibration</u>			
<i>B</i>		First Order	-0.0615 ± 0.0024	
<i>V</i>		First Order	-0.0346 ± 0.0024	
<i>I</i>		First Order	0.0332 ± 0.0113	
		Second Order	-0.0373 ± 0.0065	

**Figure 2.** Residuals (in the sense of our observed values minus the standard values) from the calibration of secondary photometric standards in M67 versus magnitude (top row), color (middle row), and color residuals versus color (bottom row).

(which Montgomery et al. used in calibrating their photometry), the agreement is fairly good (although there are significant zero-point offsets). However, outside of that range, the color-dependent residuals become noticeable, and there is a clear color-dependent trend in the $(V-I)$ residuals. Because both our primary and secondary standards covered colors up to $(V-I) \approx 1.5$, we believe our photometry should be more reliable.

**Figure 3.** Residuals (in the sense of our observed values minus the published values) from the comparison of calibrated M67 photometry with the study of Joner & Taylor (1990). Also included are the median residual values and in parentheses the semi-interquartile range (a measure of dispersion).

3 THE SINGLE-STAR SEQUENCE AND FIDUCIAL LINE

For the best possible comparison with theoretical isochrones, we would ideally like to identify a sample of unambiguous single-star cluster members that have been able to evolve without having undergone strong interactions with their neighbors. We will refer to the locus of the positions of these stars in the color-magnitude diagram (CMD) as the single-star sequence (SSS). To define such a sequence, contaminants in the CMD have to be removed. For a relatively sparse cluster like M67, this task is particularly important, so we describe our selection criteria in detail below.

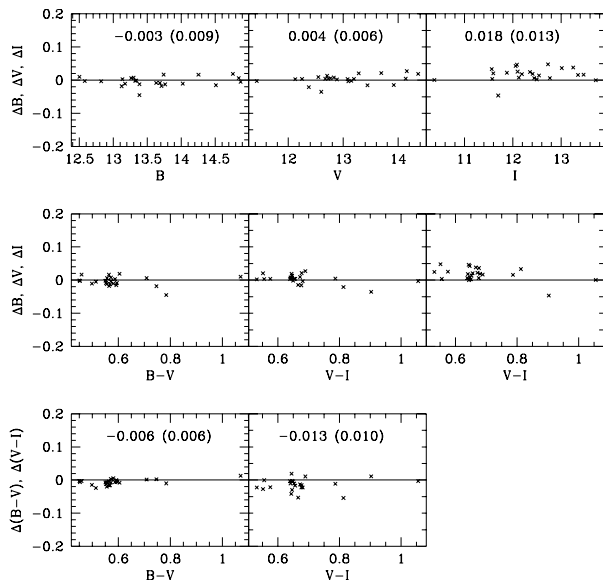


Figure 4. Residuals (in the sense of our observed values minus the published values) from the comparison of calibrated M67 photometry with the study of Chevalier & Ilovaisky (1991).

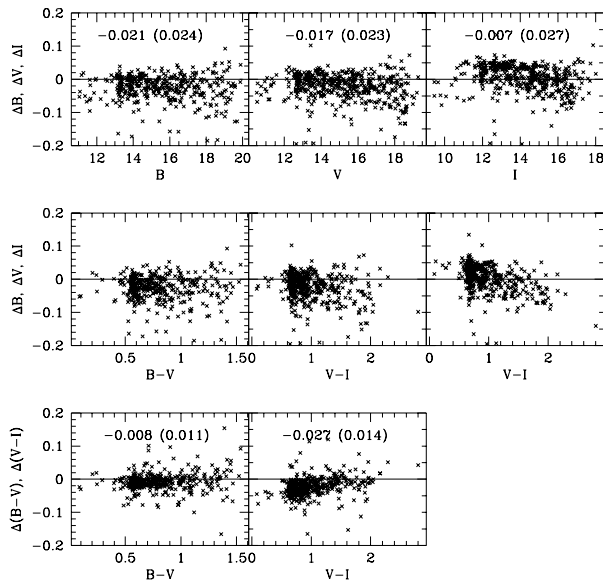


Figure 5. Residuals (in the sense of our observed values minus the published values) from the comparison of calibrated M67 photometry with the study of Montgomery et al. (1993).

3.1 Selection Criteria

The primary source of contamination in the CMD on the lower main sequence is from field stars. We have used proper motion membership probabilities from Sanders (1977) and Girard et al. (1989) for guidance where possible. Both studies had a faint limit of $V \approx 16$, although we believe that the membership probabilities for the fainter stars in the Sanders

sample may be systematically underestimated, as we found that an abnormally large number of stars with excellent VI data clearly falling on the main sequence (as delineated by other higher probability members) had low membership probabilities (see Fig. 6). In particular, there are a large number of low-probability members that fall near the main sequence having $15.2 < V < 16$. This seems to be the case for the Girard et al. dataset to a similar degree, so we will not rely entirely on the proper motions for faint stars except when both studies agree that a star is a member.

Due to the high binary content of M67 (Montgomery et al. 1993; Fan et al. 1996), attention has to be paid to contamination of the CMD by multiple star systems. We conducted a literature search for confirmed star systems among the cluster members, and found that the elimination of these systems from the CMD clarifies the position of the SSS near the cluster turnoff (TO), subgiant branch (SGB), and lower red giant branch (RGB). Known multiple star systems are identified in Table 3 along with the most recent orbit information available and photometry from this study, Montgomery et al. (1993) (for S1040, S1113, S1195, and S1250), or Stassun et al. (2002) (for S1508).

Elimination of known binaries will of course not eliminate all such systems due to observational limitations (particularly for the radial velocity surveys) and to selection effects (like those against binaries with low mass ratios or long periods). Thus, it is necessary to fall back on CMD position selection. Because of the high relative precision of the photometry for most stars in our study, we are able to eliminate from consideration stars that are likely to be unresolved binaries. However, as these cuts may not be restrictive enough in removing unresolved binaries with the lowest mass ratios, we have also used the data of Fan et al. (1996) for an additional cut. Since faint secondary stars can have significant effects on the color of a system in spite of faintness, we have examined the position of our selected stars in the CMD using several color indices. A significant shift in position relative to other stars near the SSS is an indication of an unresolved secondary star. This method works best if measurement scatter is small, which is happily the case for a subset of the filter bands used in the Fan et al. (1996) study (specifically, the filters centered at 3890, 6075, and 9190 Å).

In different portions of the CMD, slightly different criteria were used to select the stars that were most likely to be part of the SSS. These criteria were based on the direction a single star is likely to be displaced in the CMD if another single star was placed in an unresolved binary with it. Fig. 7 shows examples of this for various places on the VI fiducial line. To create this plot, we combine the V and I fluxes of a given fiducial point with that of each fainter fiducial point in order to determine where unresolved binaries would fall. The indication is that for all points up to the bottom of the turnoff gap ($12.9 < V < 13.3$) a “bluest member” selection criterion is appropriate since there is no possibility of an unresolved binary falling exactly on the SSS. For all but the bluest portion of the subgiant branch, a “faintest member” criterion is appropriate. For the red giant branch, a “reddest member” criterion works except on the lower RGB where it is possible to have a very slight red increment added if a secondary star is among the brightest main sequence stars redder than the giant primary. (We have found at least one

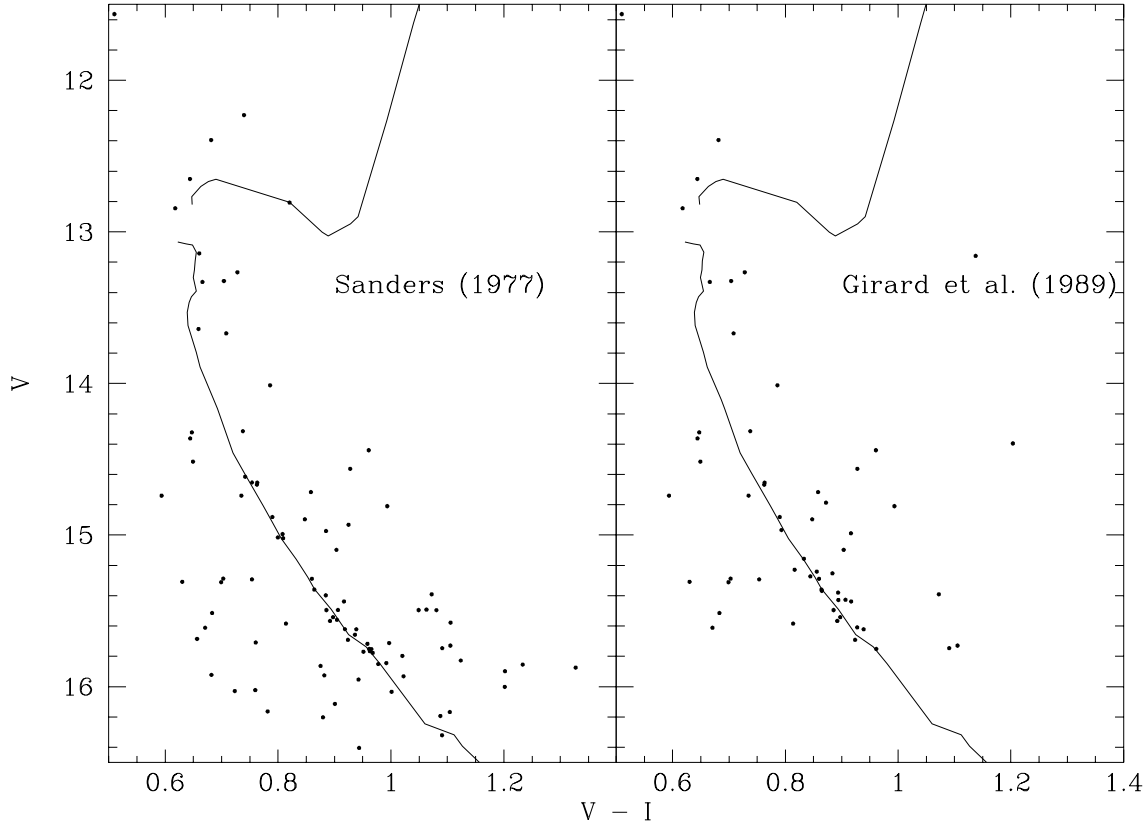


Figure 6. CMD of cluster non-members (membership probability $< 50\%$) according to proper motion studies. The photometry is from this study.

example of this in our dataset; see §3.3.3) So, it is only the bluest portion of the subgiant branch where there is likely to be significant contamination from unresolved blends with main sequence stars.

It is also possible that white dwarfs might be present in binary stars, which would result in a displacement of the system’s properties to the blue of the main sequence as shown in Fig. 8. The white dwarf photometry values were taken from the $\log g = 8$ pure hydrogen atmosphere models of Bergeron, Wesemael, & Beauchamp (1995) for $T_{\text{eff}} \leq 10^5$ K. The displacement only begins to become important for main sequence stars fainter than the turnoff. Blends with white dwarfs should have negligible effects on the determined position of the lower main sequence as they would most likely be rejected as apparent field stars on the basis of their CMD position. If they are common enough in binaries with stars on the upper main sequence, they would produce systems in the CMD that appear to be slightly (~ 0.01 mag in color) to the blue of the main sequence. This is one good reason for retaining some skepticism about using a “bluest member” selection criterion here.

Strong interactions between stars can produce systems that do not follow blend sequences. Blue stragglers are a notable example of a group of stars that can fall between the SSS and the zero-age main sequence because the hydrogen content in the stellar core is larger than expected

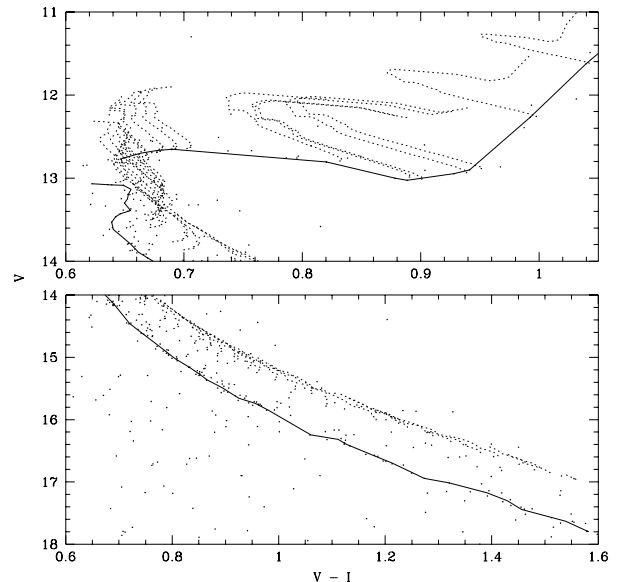


Figure 7. CMDs showing our derived fiducial line (solid line), two-star blend sequences for many different single star primaries (dotted lines), and our cluster photometry (points).

Table 3. Known Multiple Star Systems in M67

ID	V	$V - I$	P (d)	e	Ref.
EU Cnc			0.09	0.	6
III-79	15.87	1.26	0.2704	0	6
S757	13.49	0.67	0.35967	0	5
S1282	13.44	0.67	0.360452	0	7
S1036	12.80	0.59	0.441437	0	5
S1082	11.19	0.53	1.067797	0	2
S972	15.39	1.07	1.166412	0.01	10
S1077	12.61	0.81	1.358766	0.10	7
S1019	14.26	0.89	1.36022	0.02	7
S1070	13.93	0.73	2.66	0	10
S1113	13.77		2.823094	0	8
S1234	12.62	0.66	4.18258	0.26	1
S1024	12.71	0.65	7.15961	0	4
S1045	12.56	0.67	7.6452	0	4
S999	12.60	0.90	10.0553	0	4
S986	12.73	0.64	10.33813	0	3
S1272	12.54	0.66	11.0215	0.26	4
S2206	12.38	0.81	18.377	0.34	4
S1063	13.52	0.65	18.396	0.21	8
S1508	13.45	1.31	25.866	0.44	4
S821	12.79	0.68	26.259	0.4	9
S1242	12.67	0.76	31.780	0.66	4
S1040	11.52	0.91	42.877	0.	4
S1216	12.67	0.65	60.445	0.45	4
S1053	12.23	0.74	123.39	0.49	4, mem?
S1285	12.51	0.73	277.8	0.19	4
S1264a	12.05	1.03	353.9	0.38	4
S1000	12.81	0.82	531	0.09	4, nm
S1237	10.73	0.96	697.8	0.11	4
S1267	10.91	0.24	850	0.47	1
S251			948	0.55	4
S760	13.29	0.68	954	0.43	7
S752	11.32	0.33	1013	0.27	1
S1195	12.28	0.50	1139	0.03	1
S975	11.04	0.49	1231	0.12	1
S1182			1233	0.13	4
S440			1315	0.15	4
S1072	11.30	0.71	1495	0.32	4
S1250	9.69	1.33	4410	0.50	4
S997	12.13	0.56	5153	0.36	1
S1221	10.74	1.09	6445	0	4

Notes: mem?: questionable cluster member; nm: low membership probability

References: 1: Sandquist et al. 2003a; 2: van den Berg et al. 2001; 3: Sandquist & Shetrone 2003c; 4: Mathieu, Latham, & Griffin 1990; 5: Sandquist & Shetrone 2003b; 6: Gilliland et al. 1991; 7: van den Berg et al. 2002; 8: Mathieu et al. 2003; 9: Shetrone & Sandquist 2000; 10: Belloni et al. 1998

for an isolated single star of near-turnoff mass. The current leading explanations for blue stragglers are earlier episodes of binary mass transfer or stellar collisions. Blue stragglers that fall near the turnoff in the CMD can be difficult to remove. In some cases a second star will be present that still contributes enough to the system flux (whether a left-over donor star or a star that was captured into a bound orbit during a multiple star interaction) that the star will be clearly separated from the single-star sequence. In other cases, radial velocity studies (Mathieu et al. 1986) can eliminate some systems even if the secondary is undetectable on its own.

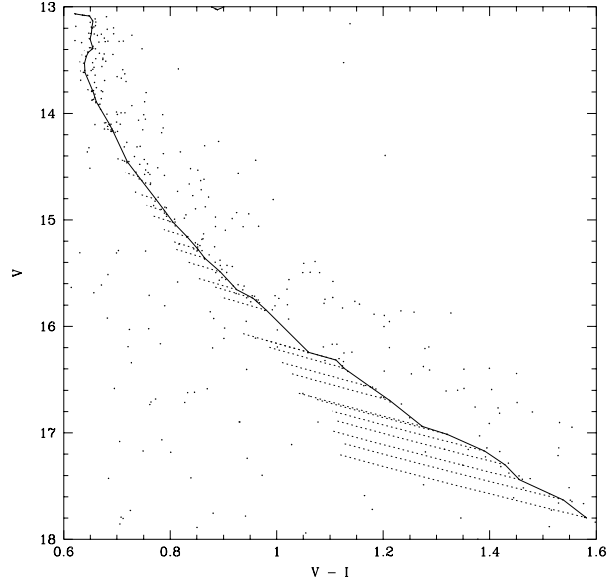


Figure 8. CMDs showing our derived fiducial line (*solid line*), two star blend sequences for unseen white dwarf companions (*dotted lines*) using the sequences of Bergeron, Wesemael, & Beauchamp (1995), and our cluster photometry (*points*).

Three examples of interacting W UMa variable stars fall near the M67 turnoff, but it is unlikely that stars of this type will be a significant contaminant because they are usually easily identified from photometric studies like the ones carried out by Stassun et al. (2002) and Sandquist & Shetrone (2003b) unless the system has a low inclination. Such systems generally will not have system photometry that moves them bluer than the single-star sequence (Rucinski & Duerbeck 1997) unless one of the stars was already a blue straggler when strong interactions began. However, we do have to be aware that there is a small probability that a blue straggler or interacting star could fall near the SSS.

In a small number of cases we have also eliminated stars that appear to be low amplitude variable stars. With a large number of observations, it should in principle be possible to determine an accurate median magnitude for stars that vary on fairly short time-scales ($P \lesssim 10$ d). In some cases variability will be related to binary interactions or to rotational modulation of star spots. In either case, the variability can introduce enough uncertainty that it could affect the position of the star in the CMD. We have used our time-series photometry and the study of Stassun et al. (2002) to identify and remove these stars. We confirm low amplitude variability of the stars S974 and S1093 detected by Stassun et al., and in addition find that S1042 also appears to be variable (although Sanders 1977 gives it a 0% membership probability). In addition, although S1112 made it through our other cuts, it was shown in van den Berg et al. (2002) to be a low-amplitude variable, and so was eliminated.

3.2 Other Means of Broadening the SSS

In using the above criteria to select single stars, we may introduce some bias into our sample because other factors can lead to a broadening of the region of the CMD containing single stars. Factors include differences in age, chemical composition, and angular momentum. We will briefly discuss these below.

For a cluster as old as M67, differences in age due to variations in the time of formation result in relatively small differences in CMD position. The effects are maximized for the most evolved stars in the cluster. Our selection criteria would tend to bias us toward selecting the oldest stars in the cluster on the upper main sequence, SGB, and RGB. Age spreads in young open clusters are typically found to be less than 10 Myr (e.g. Belikov et al. 2000; Soderblom et al. 1999; Baume, Vázquez, & Feinstein 1999). From isochrones (Yi et al. 2001), we find that such an age difference would cause a color shift of only about 0.001 in $V - I$ at the turnoff, and about 0.004 mag in V on the subgiant branch. On this basis, we neglect further discussion of age spreads.

Composition differences can also create differences in properties among stars of the same age and mass. There are no large spectroscopic studies of M67 to give us an accurate measure of how much of an intrinsic scatter in $[\text{Fe}/\text{H}]$ there might be in the cluster. Indications from 4 stars observed by Shetrone & Sandquist (2000) are that the scatter among main sequence stars is less than 0.10 dex. Observations of 16 dwarfs in the Pleiades by Wilden et al. (2002) indicated deviations from the mean of less than 0.03 dex. At the turnoff, a 0.1 dex difference in $[\text{Fe}/\text{H}]$ would result in a small change in the shape of the sequence, a change in turnoff color by a little over 0.01, and a change in V by almost 0.1 mag. The slope of the SGB is also affected, resulting in the largest differences at the red end of around 0.2 mag in V . Our selection criteria would tend to be biased toward the stars with the lowest metallicity values on the main sequence, but the highest metallicity stars on the SGB and RGB. Although this bias could potentially affect the shape of single star sequence, we will not discuss this further because there is as yet no evidence of significant metallicity scatter. We will discuss the possibility of evolution-driven composition effects in §3.3.3.

Star-to-star angular momentum differences are believed to affect main sequence Li abundances (e.g. Jones, Fischer, & Soderblom 1999), although the most abundant chemical species are not significantly affected. Changes in CMD position on the main sequence are thus not likely to result from the composition changes. Observations of $v_{\text{rot}} \sin i$ for M67 stars show values of less than 8 km s⁻¹ (Melo et al. 2001). These low rotation rates are not likely to affect the stellar structure enough to move the star significantly in the CMD. As a result, we will drop further discussion of angular momentum effects.

3.3 Selected Stars and the SSS

We determined main sequence fiducial points using our calibrated ensemble photometry. In places (particularly on the subgiant branch and above), individual stars were used to define the SSS if we deemed that there was sufficient evidence to support this. In places where there were more than

Table 4. VI Fiducial Points for M67

V	$V - I$	N
11.4291	1.0557	1
11.6221	1.0400	1
12.2669	0.9926	1
12.9001	0.9414	1
12.9475	0.9281	1
13.0265	0.8886	1
13.0015	0.8782	1
12.8059	0.8203	1
12.6539	0.6899	2
12.6677	0.6768	3
12.7012	0.6634	2
12.7677	0.6470	3
12.8189	0.6479	4
13.0667	0.6222	1
13.0791	0.6370	2
13.0861	0.6487	1
13.1333	0.6552	3
13.1907	0.6530	3
13.2516	0.6520	2
13.3012	0.6497	1
13.3908	0.6549	5
13.4271	0.6462	1
13.4651	0.6423	1
13.5305	0.6388	1
13.6178	0.6402	3
13.7941	0.6549	4
13.8925	0.6616	7
14.1064	0.6862	4
14.1657	0.6925	6
14.4573	0.7199	3
14.5950	0.7407	3
14.8078	0.7736	3
14.9184	0.7902	5
15.0238	0.8057	4
15.1593	0.8319	2
15.2770	0.8526	6
15.3586	0.8648	3
15.4896	0.8943	9
15.6565	0.9250	3
15.7368	0.9558	8
15.8492	0.9803	2
16.2449	1.0603	2
16.3165	1.1117	3
16.3931	1.1265	3
16.5692	1.1762	3
16.6970	1.2128	4
16.9410	1.2737	1
17.0145	1.3203	1
17.1726	1.3907	4
17.3017	1.4294	2
17.4407	1.4562	5
17.6307	1.5382	5
17.7996	1.5821	3

one star clumped together in the CMD, calculated fiducial points were weighted averages of photometric values for the group. Our fiducial points are presented in Table 4, including the number of stars N used to compute each point.

We truncate our tabulated sequence at $V \approx 17.8$ because this corresponds to a color at the red end of the range covered by our calibrating secondary standards. However, we are able to identify additional stars that form an extension of

the main sequence. Our selected stars are presented in Table 5. Columns 1 – 3 contain identification numbers from Sanders (1977), Montgomery et al. (1993), and Fan et al. (1996), columns 4 – 9 contain the photometry and numbers of observations in each filter band, and columns 10 and 11 contain proper motion membership probabilities from Sanders (1977) and Girard et al. (1989). (Note that we tabulate magnitudes and colors to fractions of millimag because in many cases the *relative* accuracies justify this. The possibility of calibration errors means that these could deviate from the true photometry values on an *absolute* scale.) A subset of stars had questionable values resulting from small numbers of measurements, contamination due to light from nearby stars, or instrumental problems. If the star falls near the apparent position of the SSS we include it in the table for possible future use, and note it with an “a”. We are confident in our choices for the SSS based on the degree to which stars in our data and that of Fan et al. (1996) fall in the same regions of the CMD, as can be seen in Figs. 9, 10, and 12 below.

In addition we identify an alternate sequence of main sequence stars that fall at the blue end of the color distribution at each magnitude level. If our magnitudes are mostly free of systematic errors and our error estimates reflect the real uncertainty in measurements relative to other stars, then these stars would most accurately delineate the SSS. The stars in this sequence are notated with a “b” in Table 5. In most cases, the difference in color between this bluer sequence and the average sequence is no more than 0.02 in $V - I$.

Finally, in Table 6, we identify stars that are worthy of further study. We have identified several stars on the RGB that are likely to be part of binary systems, several new blue straggler star (BSS) candidates, and possible triple systems.

3.3.1 The Upper Red Giant Branch (RGB)

The observations made by us and by Fan et al. were generally long enough that stars on the upper giant branch were saturated on the CCD, and so were not measured by either study. However, Janes & Smith (1984) studied the upper giant branch to try and sort first-ascent giant stars from stars in later evolutionary phases and star in binaries. Montgomery et al. (1993) tabulate photometry for the brightest stars taken from other studies. Because there are likely to be systematic errors resulting from differences in calibration, we do not include these stars in Table 5. However, the stars that are most likely to be on the SSS (in order from RGB tip faintward) are S1553 (61%), S488 (51%), S1135 (19%), S978 (99%; 95%), S364 (82%), S1557 (77%), and S1016 (98%; 93%). The percentages quoted are proper motion membership probabilities from Sanders (1977) and Girard et al. (1989) if available. All of these stars are high probability proper motion and radial velocity members (Mathieu et al. 1986) with the exception of S1135, which is a high-probability radial velocity member.

3.3.2 The Red Giant Clump

We were able to photometer 4 stars falling in the red giant clump (see Table 5), and identify 3 others (S1316, S1479, and

S1592) from the Montgomery et al. (1993) listing of bright stars. All are high probability proper motion and radial velocity members of M67.

3.3.3 The Lower Giant Branch

We selected giant branch members based on whether they seemed to be closest to a lower envelope of stars leading up the RGB. In many cases, cluster members fall near, but not on the giant branch. While some of these are to the blue of the giant branch (and thus are very likely to be binary stars), there are several stars to the *red* of the giant branch. Among the bluer stars are known binaries like S1040, S1182, S1195, S1221, and S1237. We also identify S721, S1054, S1254, and S1288 as probable binaries based on their colors from our data and Fan et al. (1996) data. We also reject S1293 as too blue in our data, although it appears to lie on the giant branch in the Fan et al. data. CMDs are shown in Fig. 9.

As mentioned earlier, systems can be created with colors *redward* of the giant branch if a main sequence secondary star with a color redder than the giant star is present. S1001 is one example that appears redward of the giant branch by a small but noticeable amount in all of the colors we examined, so that it was not included in the SSS. The fainter the giant star is, the larger the red deviation caused by a main sequence companion can be. S794 is an example of this near the base of the red giant branch. S1463 is another high probability cluster member nearby in the CMD that deviates by an amount that *cannot* be explained by a single main sequence companion.

One can also question whether surface composition changes driven by evolutionary changes at first dredge-up on the RGB might significantly affect the CMD position of stars in this section. This is only likely to be a significant worry if different M67 giants undergo the dredge-up event at substantially different positions on the RGB or if there is scatter in the amount of material dredged up. Brown (1987) examined C and N abundances along the giant branch, and found a fairly abrupt change in $12.2 < V < 13$. Gilroy & Brown (1991) examined $^{12}\text{C} / ^{13}\text{C}$ ratios, and found them varying in the same range. This is partly because there are few stars in this portion of the CMD (see Fig. 9). In fact, we rejected only three stars in this range: S794, S1001, and S1463. S794 was observed by Gilroy & Brown though, and seems to have abundances consistent with not yet having undergone dredge-up. S1463 was also observed, but its values were inconclusive. However, Balachandran (1995) detected Li in the star, which is unusual because none of the other stars in similar evolutionary stages have detectable Li. We believe this spectroscopic evidence strongly supports the exclusion of S794 and S1463 from the SSS. S1001 remains a marginal case.

3.3.4 The Subgiant Branch (SGB)

We define this region to be between the base of RGB (the local minimum in luminosity) and the top of the main sequence (the local maximum). A close examination of the $(m_{3890}, m_{3890} - m_{9190})$ CMD from Fan et al. (1996) reveals a well-defined string of stars delineating the SGB. In the $(m_{6075}, m_{3890} - m_{6075})$ CMD, there are clearly a small number of stars that are fainter than the rest. There is one

Table 5. High-Probability Single Stars in M67

Sanders	MMJ	Fan	V	N_V	$V - I$	N_I	$B - V$	N_B	P_S	P_G	Notes
<u>Clump Stars</u>											
1010	6485	3536	10.4675 ± 0.0005	1711	1.0737 ± 0.0020	190	1.0946 ± 0.0032	62	0.96	0.99	
1074	6492	3204	10.5221 ± 0.0005	1991	1.0721 ± 0.0019	144	1.0924 ± 0.0019	62	0.91	0.98	
1084	6494	3642	10.4929 ± 0.0004	2158	1.0547 ± 0.0020	134	1.0855 ± 0.0022	62	0.92	0.98	
1279	6503	3726	10.5379 ± 0.0003	1814	1.0859 ± 0.0012	191	1.1144 ± 0.0020	62	0.92	0.99	
1316	6506	4159							0.99	0.95	
1479	6512	4611							0.98	0.95	
1592	6516	5050							0.97	0.92	
<u>Lower Giant Branch</u>											
989		3492	11.4291 ± 0.0003	2148	1.0557 ± 0.0006	564	1.0702 ± 0.0199	62	0.95	0.99	
1277	6502	4117	11.6221 ± 0.0005	1240	1.0400 ± 0.0006	392	1.0367 ± 0.0025	62	0.95	0.98	
1305	5997	3949	12.2669 ± 0.0003	2446	0.9926 ± 0.0005	668	0.9812 ± 0.0018	62	0.95	0.99	
1231	5855	3736	12.9001 ± 0.0004	2150	0.9414 ± 0.0005	815	0.9179 ± 0.0035	62	0.95	0.98	
606	5059	2210							0.96	0.98	
1103	5663	3413							0.95	0.99	
1402	6508	4878							0.83	0.77	
1585		5191							0.89	0.91	
<u>Subgiant Branch</u>											
1245	6114	4178	12.9475 ± 0.0008	922	0.9281 ± 0.0012	362	0.8925 ± 0.0031	56	0.95	0.98	<i>a</i>
1060	5651	3406	13.0265 ± 0.0006	2449	0.8886 ± 0.0007	819	0.8545 ± 0.0023	62	0.96	0.98	<i>a</i>
1056	5580	3296	13.0015 ± 0.0005	2394	0.8782 ± 0.0006	820	0.8379 ± 0.0027	62	0.95	0.96	<i>a</i>
1323	5996	3935	12.8059 ± 0.0012	491	0.8203 ± 0.0086	8		0	0.95	0.99	<i>a</i>
756	5388	2932	12.6546 ± 0.0007	2015	0.6903 ± 0.0009	810	0.6128 ± 0.0319	62	0.96	0.99	<i>a</i>
775	5371	2887	12.6526 ± 0.0010	1877	0.6892 ± 0.0011	818	0.6130 ± 0.0025	62	0.84	0.99	<i>a</i>
1034	5644	3395	12.6530 ± 0.0003	2011	0.6790 ± 0.0004	819	0.6056 ± 0.0011	62	0.95	0.99	<i>a</i>
1270	6166	4314	12.6843 ± 0.0013	589	0.6771 ± 0.0034	181	0.5578 ± 0.0069	27	0.94	0.99	
2212	5884	3781	12.6922 ± 0.0004	2011	0.6728 ± 0.0006	819	0.5869 ± 0.0016	62	0.95	0.99	
598	5041	2172							0.96	0.99	
859		2481							0.89	0.97	
1268	6177	4335							0.94	0.99	
1274	5925	3836							0.93	0.99	
<u>The Turnoff</u>											
1456	6224	4434	12.7160 ± 0.0008	335	0.6619 ± 0.0023	106	0.5181 ± 0.0074	25	0.94	0.99	
	5951	3874	12.6825 ± 0.0009	1593	0.6637 ± 0.0010	798	0.5806 ± 0.0039	62			<i>a</i>
995	5675	3454	12.7702 ± 0.0002	2015	0.6463 ± 0.0004	815	0.5501 ± 0.0027	62	0.82	0.99	<i>a</i>
1083	5825	3686	12.7547 ± 0.0004	2448	0.6495 ± 0.0005	672	0.5678 ± 0.0016	62	0.95	0.99	
1310	6077	4091	12.7792 ± 0.0008	1510	0.6358 ± 0.0016	478	0.5601 ± 0.0026	61	0.93	0.99	
1003	5562	3267	12.8281 ± 0.0005	2008	0.6407 ± 0.0007	814	0.5550 ± 0.0032	62	0.91	0.99	<i>a</i>
1049	5573	3283	12.8098 ± 0.0005	2045	0.6422 ± 0.0006	816	0.5552 ± 0.0029	62	0.95	0.98	<i>a</i>
1071	5842	3708	12.8111 ± 0.0003	2436	0.6511 ± 0.0006	673	0.5639 ± 0.0037	62	0.94	0.98	
1076	5586	3302	12.8266 ± 0.0003	2416	0.6525 ± 0.0005	669	0.5571 ± 0.0016	62	0.94	0.98	
926		3632							0.94	0.98	
1589		5052							0.94	0.98	
1639		5318							0.90	0.95	
<u>Lower Turnoff</u>											
731	5335	2841							0.96	0.98	
1230	6103	4153	13.0667 ± 0.0016	1219	0.6222 ± 0.0018	470	0.5364 ± 0.0028	52	0.94	0.99	<i>a</i>
998	5610	3359	13.0803 ± 0.0004	2013	0.6389 ± 0.0006	816	0.5522 ± 0.0027	62	0.95	0.99	<i>a</i>
1302	5926	3832	13.0779 ± 0.0004	2403	0.6356 ± 0.0006	669	0.5605 ± 0.0037	62	0.95	0.97	<i>a</i>
745	5169	2461	13.0861 ± 0.0007	849	0.6487 ± 0.0041	29		0	0.96	0.99	<i>a</i>
827	5312	2765							0.95	0.95	
1219	5863	3766	13.1130 ± 0.0005	1703	0.6590 ± 0.0008	747	0.5725 ± 0.0020	61	0.93	0.99	
2205	5679	3458	13.1453 ± 0.0004	2152	0.6498 ± 0.0008	809	0.5642 ± 0.0056	62	0.51	0.98	<i>a</i>
2220	5597	3335	13.1424 ± 0.0012	2041	0.6603 ± 0.0016	812	0.5882 ± 0.0025	62	0.04	0.99	
994	5716	3510	13.1956 ± 0.0003	2012	0.6526 ± 0.0006	810	0.5678 ± 0.0024	62	0.95	0.98	
1207	6108	4174	13.1763 ± 0.0005	744	0.6597 ± 0.0031	91	0.5349 ± 0.0561	13	0.95	0.98	
1313	6019	3977	13.1985 ± 0.0018	1430	0.6542 ± 0.0019	371	0.5660 ± 0.0065	56	0.94	0.98	
1181		4119							0.96	0.99	
1197	5959	3909							0.95	0.99	
1441	6336	4689							0.95	0.98	

Table 5 – continued

Sanders	MMJ	Fan	V	N_V	$V - I$	N_I	$B - V$	N_B	P_S	P_G	Notes
964	5622	3383	13.2544 ± 0.0004	1871	0.6574 ± 0.0009	613	0.5826 ± 0.0038	49	0.95	0.97	
1030	5803	3633	13.2471 ± 0.0005	2007	0.6470 ± 0.0009	814	0.5674 ± 0.0028	62	0.90	0.98	a
1635		5352							0.71	0.54	
1062	5733	3527	13.3012 ± 0.0004	2445	0.6497 ± 0.0006	771	0.5646 ± 0.0014	62	0.96	0.97	
1189	5900	3838							0.95	0.97	
1458	6332	4676							0.95	0.97	
648		2365							0.93	0.73	
711		2653							0.90	0.96	
723	5277	2726							0.87	0.93	
809	5314	2778	13.3839 ± 0.0006	997	0.6486 ± 0.0033	239	0.5545 ± 0.0039	25	0.94	0.96	a
967	5629	3390	13.3986 ± 0.0004	1784	0.6525 ± 0.0006	742	0.5673 ± 0.0040	49	0.94	0.99	
1017	5478	3102	13.3933 ± 0.0006	1928	0.6595 ± 0.0008	812	0.5504 ± 0.0036	62	0.95	0.97	
1240	6134	4230	13.3698 ± 0.0011	778	0.6550 ± 0.0020	322	0.5537 ± 0.0140	44	0.93	0.98	
2221	5559	3254	13.3878 ± 0.0004	2157	0.6544 ± 0.0006	813	0.5742 ± 0.0019	62	0.90	0.98	
839	5183	2463							0.85	0.84	
939	5434	3038							0.95	0.99	
990	5464	3083	13.4271 ± 0.0005	2019	0.6462 ± 0.0009	811	0.5507 ± 0.0016	53	0.93	0.97	a
740	5354	2881	13.4651 ± 0.0003	1757	0.6423 ± 0.0009	365	0.5476 ± 0.0070	25	0.87	0.98	a
784	5283	2698	13.5305 ± 0.0006	1906	0.6388 ± 0.0011	519	0.5491 ± 0.0047	35	0.91	0.99	a
1321	6127	4192	13.5674 ± 0.0021	203	0.6569 ± 0.0065	28	0.5487 ± 0.0321	13	0.94	0.98	b
763	5196	2494	13.5966 ± 0.0005	799	0.6394 ± 0.0024	143		0	0.95	0.98	
803	5301	2733	13.6420 ± 0.0005	1954	0.6449 ± 0.0009	541	0.5635 ± 0.0020	37	0.95	0.99	
1061	5546	3227	13.6147 ± 0.0005	2428	0.6370 ± 0.0008	812	0.5419 ± 0.0044	62	0.96	0.97	a
844		2526							0.92	0.97	
<u>Upper Main Sequence</u>											
1115		3097							0.91	0.95	
1281	5972	3903	13.6886 ± 0.0007	2211	0.6318 ± 0.0010	765	0.5272 ± 0.0049	60	0.90	0.99	BSS?
595		2039							0.94	0.90	
1055	5471	3080	13.7936 ± 0.0007	2298	0.6523 ± 0.0010	811	0.5679 ± 0.0029	62	0.96	0.98	a
1244	6058	4071	13.8197 ± 0.0008	1433	0.6586 ± 0.0010	643	0.5807 ± 0.0049	61	0.92	0.97	
1265	6065	4077	13.7863 ± 0.0006	1277	0.6532 ± 0.0008	636	0.5697 ± 0.0023	62	0.94	0.98	
1300	6060	4057	13.7857 ± 0.0007	1898	0.6559 ± 0.0009	648	0.5791 ± 0.0033	62	0.94	0.95	
755	5189	2491	13.8996 ± 0.0008	791	0.6601 ± 0.0020	138		0	0.96	0.98	a
796	5412	2978	13.8526 ± 0.0005	2304	0.6583 ± 0.0007	661	0.5762 ± 0.0028	62	0.92	0.98	
987	5608	3360	13.9182 ± 0.0004	2139	0.6659 ± 0.0008	805	0.5917 ± 0.0082	61	0.95	0.98	
1021	5522	3186	13.9133 ± 0.0008	1951	0.6680 ± 0.0010	805	0.5770 ± 0.0023	62	0.89	0.98	
1035	5657	3425	13.8677 ± 0.0005	1994	0.6563 ± 0.0011	810	0.5757 ± 0.0033	62	0.90	0.98	
1051	5685	3455	13.9627 ± 0.0005	2031	0.6693 ± 0.0009	805	0.5811 ± 0.0020	62	0.94	0.96	a
1075	5692	3456	13.8722 ± 0.0003	2293	0.6544 ± 0.0008	661	0.5682 ± 0.0037	62	0.93	0.97	a
647		2301							0.95	0.96	
650		1902							0.92	0.75	
1201	5989	3954							0.94	0.98	
848		2769							0.95	0.93	
1318		3960							0.86	0.90	
805	5229	2559	14.0073 ± 0.0006	1107	0.6812 ± 0.0018	187		0	0.95	0.93	b
1446	6395	4842							0.94	0.74	
1406	6237	4479							0.85	0.96	
1330	6104	4132							0.79	0.82	
603	5111	2305							0.93	0.97	
744	5181	2484	14.1219 ± 0.0009	860	0.6824 ± 0.0026	110		0	0.95	0.79	a
788	5305	2746	14.1117 ± 0.0008	1947	0.6867 ± 0.0012	539	0.6077 ± 0.0030	37	0.95	0.97	
1213	6031	4020	14.0869 ± 0.0015	1857	0.6791 ± 0.0017	466	0.5995 ± 0.0057	40	0.96	0.98	a
1283	5873	3758	14.1018 ± 0.0005	2396	0.6888 ± 0.0010	801	0.6207 ± 0.0030	60	0.96	0.96	
722	5307	2781							0.96	0.90	
1107	5722	3491							0.73	0.96	
982	5776	3608	14.1056 ± 0.0004	2132	0.6586 ± 0.0007	784	0.5943 ± 0.0050	60	0.93	0.94	b
1033	5567	3274	14.1553 ± 0.0005	1993	0.6888 ± 0.0008	803	0.6039 ± 0.0051	62	0.91	0.97	a
1078	5826	3687	14.1781 ± 0.0005	2391	0.6966 ± 0.0009	660	0.6281 ± 0.0046	61	0.85	0.97	
1087	5753	3551	14.1697 ± 0.0006	2272	0.6888 ± 0.0008	658	0.6217 ± 0.0034	58	0.79	0.84	a
1089	5532	3191	14.1695 ± 0.0006	1799	0.7010 ± 0.0008	525	0.6217 ± 0.0023	59	0.91	0.91	
1248	5963	3896	14.1694 ± 0.0004	1988	0.6903 ± 0.0006	758	0.6216 ± 0.0045	60	0.93	0.96	

Table 5 – *continued*

Sanders	MMJ	Fan	V	N_V	$V - I$	N_I	$B - V$	N_B	P_S	P_G	Notes
1260	5937	3855	14.1471 ± 0.0006	1980	0.6909 ± 0.0009	799	0.6117 ± 0.0056	62	0.91	0.97	
728	5294	2752							0.94	0.76	
937	5426	3031							0.96	0.95	
1505		4656							0.94	0.79	
630		2024							0.96	0.91	
1426	6405	4887							0.95	0.91	
1102	5479	3092							0.95	0.86	
829	5338	2806							0.94	0.91	
1423	6241	4478							0.89	0.88	
1449	6265	4515							0.85	0.96	
958		3249	14.4493 ± 0.0009	874	0.7143 ± 0.0021	257		0	0.92	0.96	
966	5704	3503	14.4644 ± 0.0006	1651	0.7187 ± 0.0010	693	0.6607 ± 0.0033	46	0.87	0.77	<i>a</i>
1255	5995	3953	14.4525 ± 0.0007	1972	0.7224 ± 0.0010	719	0.6631 ± 0.0056	61	0.86	0.94	
1096	5541	3210	14.4743 ± 0.0115	235	0.7573 ± 0.0118	28		0	0.90	0.94	<i>b</i>
1258		4309	14.4788 ± 0.0012	584	0.7428 ± 0.0020	213	0.6323 ± 0.0307	24	0.96	0.92	<i>b</i>
621	5039	2146							0.95	0.87	
942	5444	3059							0.95	0.90	
1421		4446							0.81	0.80	
1616	6460	4983							0.95	0.85	
945	5744	3570							0.94	0.93	
724		3017							0.96	0.93	
1452	6347	4706							0.95	0.86	
753	5243	2625	14.6158 ± 0.0005	1328	0.7418 ± 0.0012	381	0.6790 ± 0.0027	34	0.46	0.93	<i>a</i>
770	5357	2867	14.6296 ± 0.0010	1829	0.7466 ± 0.0013	791	0.6748 ± 0.0044	60	0.93	0.88	
1218	5966	3910	14.5525 ± 0.0006	1638	0.7357 ± 0.0011	682	0.6731 ± 0.0043	61	0.93	0.97	
779	5306	2758							0.93	0.85	
951	5489	3141							0.94	0.87	
1184		3937							0.94	0.87	
2211	6387	4820							0.58	0.76	
1341	5908	3789							0.83	0.94	
1106	5469	3056							0.87	0.91	
629	5089	2251							0.42	0.73	
955		3309							0.85	0.74	
928		3104							0.86	0.74	
785	5346	2845	14.8244 ± 0.0010	2217	0.7715 ± 0.0013	736	0.7212 ± 0.0073	53	0.95	0.88	<i>a</i>
802	5360	2866	14.7875 ± 0.0006	2260	0.7774 ± 0.0012	651	0.7230 ± 0.0076	58	0.96	0.86	
2213	5517	3181	14.8653 ± 0.0012	1903	0.7689 ± 0.0018	789	0.7105 ± 0.0089	59	0.95	0.57	
640		1872							0.51	0.63	
754	5372	2901	14.9665 ± 0.0011	1923	0.7932 ± 0.0014	780	0.7431 ± 0.0064	59	0.83	0.47	<i>a</i>
1004	5768	3589	14.9470 ± 0.0008	1957	0.7929 ± 0.0011	790	0.7377 ± 0.0055	59	0.94	0.89	
1067	5455	3043	14.9005 ± 0.0007	2287	0.7832 ± 0.0011	716	0.7253 ± 0.0057	58	0.60	0.62	<i>a</i>
1269	6080	4106	14.9361 ± 0.0010	1207	0.7892 ± 0.0016	567	0.7428 ± 0.0050	58	0.94	0.81	<i>a</i>
1289	5879	3768	14.8864 ± 0.0007	2376	0.7927 ± 0.0011	787	0.7513 ± 0.0040	60	0.90	0.94	
820	5310	2767	14.9838 ± 0.0020	459	0.8266 ± 0.0061	26		0	0.95	0.77	<i>b</i>
795	5391	2928	14.9935 ± 0.0009	2224	0.8081 ± 0.0013	647	0.7457 ± 0.0059	53	0.42	0.62	
799	5297	2729	15.0205 ± 0.0007	1896	0.8091 ± 0.0014	518	0.7581 ± 0.0048	37	0.23	0.83	
801	5424	3002	15.0563 ± 0.0007	2269	0.8095 ± 0.0011	641	0.7486 ± 0.0101	56	0.95	0.87	
1068	5578	3287	15.0158 ± 0.0006	2354	0.7995 ± 0.0010	703	0.7469 ± 0.0073	53	0.24	0.83	<i>a</i>
772	5269	2663	15.1563 ± 0.0007	1353	0.8330 ± 0.0015	409	0.7677 ± 0.0040	35	0.91	0.49	
1307	5949	3864	15.1615 ± 0.0006	2370	0.8310 ± 0.0013	642	0.7799 ± 0.0096	54	0.94	0.80	
941	5771	3614							0.94	0.69	
1029	5709	3495	15.2151 ± 0.0012	1929	0.8472 ± 0.0018	778	0.7795 ± 0.0096	52	0.83	0.72	
1079	5725	3505	15.2860 ± 0.0008	2308	0.8520 ± 0.0020	635	0.8073 ± 0.0042	51	0.94	0.63	
1090	5526	3183	15.2722 ± 0.0009	1408	0.8444 ± 0.0024	397	0.7792 ± 0.0050	36	0.53	0.47	<i>a</i>
1217	6161	4311	15.2415 ± 0.0021	282	0.8558 ± 0.0043	147		0	0.93	0.38	
1227	6046	4046	15.2888 ± 0.0008	1776	0.8598 ± 0.0013	628	0.8208 ± 0.0070	51	0.00	0.32	
1291		3926	15.2926 ± 0.0008	2326	0.8502 ± 0.0014	724	0.8150 ± 0.0068	57	0.94	0.78	<i>a</i>
1469	6321	4633							0.94	0.23	
626		1947							0.67	0.42	
1100	5560	3238	15.2300 ± 0.0214	213	0.8516 ± 0.0219	27		0	0.81	0.61	<i>b</i>
1212	6139	4248	15.2550 ± 0.0015	643	0.8516 ± 0.0137	117		0	0.63	0.83	<i>b</i>
2202	5551	3256	15.2289 ± 0.0017		0.8166 ± 0.0032		0.7787 ± 0.0272		0.74	0.47	<i>b</i>

Table 5 – *continued*

Sanders	MMJ	Fan	V	N_V	$V - I$	N_I	$B - V$	N_B	P_S	P_G	Notes
611	5090	2265							0.92	0.76	
778	5265	2657	15.3595 ± 0.0007	1340	0.8642 ± 0.0015	398	0.8108 ± 0.0060	34	0.00	0.28	<i>a</i>
804	5186	2477	15.3282 ± 0.0018	787	0.8731 ± 0.0048	110		0	0.95	0.57	
993	5441	3037	15.3678 ± 0.0011	1839	0.8647 ± 0.0016	774	0.8105 ± 0.0059	44	0.88	0.44	<i>a</i>
1028	5563	3268	15.3976 ± 0.0008	1920	0.8845 ± 0.0013	778	0.8326 ± 0.0047	55	0.00	0.66	
1039	5459	3068	15.5666 ± 0.0010	1832	0.8921 ± 0.0013	770	0.8206 ± 0.0083	41	0.03	0.44	
1081	5800	3623	15.5594 ± 0.0007	2312	0.9043 ± 0.0016	632	0.8550 ± 0.0088	47	0.00	0.66	<i>a</i>
1085	5539	3208	15.5411 ± 0.0008	2159	0.8972 ± 0.0015	629	0.8448 ± 0.0096	36	0.00	0.31	<i>a</i>
1215	5841	3720	15.4271 ± 0.0009	1633	0.9067 ± 0.0014	599	0.8496 ± 0.0060	40	0.67	0.08	
1229	5904	3825	15.4645 ± 0.0006	2030	0.8971 ± 0.0010	775	0.8512 ± 0.0051	50	0.80		
1304	5924	3829	15.4284 ± 0.0009	2338	0.8941 ± 0.0015	634	0.8461 ± 0.0055	46	0.71	0.21	
1312	6015	3972	15.4940 ± 0.0020	1511	0.9061 ± 0.0027	353	0.8505 ± 0.0092	39	0.00		
1443		4440	15.3794 ± 0.0027	281	0.8936 ± 0.0047	93		0	0.94	0.16	
2215	6005	3967	15.4949 ± 0.0012	1884	0.8855 ± 0.0019	681	0.8563 ± 0.0117	49	0.01	0.41	<i>a</i>
769	5319	2807	15.6086 ± 0.0011	1636	0.9275 ± 0.0017	613	0.8502 ± 0.0048	37	0.95	0.20	
1038	5666	3438	15.6911 ± 0.0009	1885	0.9238 ± 0.0014	768	0.8620 ± 0.0073	43	0.00	0.17	<i>a</i>
1435	6214	4420	15.6206 ± 0.0034	182	0.9185 ± 0.0046	70		0	0.00		
	6102	4147	15.7126 ± 0.0016	1064	0.9540 ± 0.0026	453	0.9079 ± 0.0109	48			
	5943	3861	15.7319 ± 0.0014	1706	0.9435 ± 0.0021	758	0.8641 ± 0.0087	38			<i>a</i>
764	5317	2804	15.7170 ± 0.0010	1600	0.9584 ± 0.0018	607	0.8966 ± 0.0059	35	0.00		
811	5386	2914	15.7770 ± 0.0017	698	0.9676 ± 0.0034	273	0.9106 ± 0.0185	23	0.08		
1091	5470	3069	15.7694 ± 0.0036	470	0.9512 ± 0.0051	232	0.8783 ± 0.0133	11	0.00		<i>a</i>
1098	5513	3161	15.7514 ± 0.0068	208	0.9614 ± 0.0092	26		0	0.00	0.27	
1311	5956	3867	15.7522 ± 0.0011	1540	0.9652 ± 0.0025	351	0.9076 ± 0.0051	34	0.00		
1472	6248	4475	15.7653 ± 0.0036	166	0.9627 ± 0.0102	32		0	0.00		
960	5623	3389	15.8502 ± 0.0015	1206	0.9775 ± 0.0024	284		0	0.00		<i>a</i>
1296	6195	4357	15.8443 ± 0.0033	469	0.9918 ± 0.0050	126		0	0.00		
1315	6096	4128	15.9311 ± 0.0034	424	1.0224 ± 0.0077	30		0	0.00		<i>b</i>
1433	6229	4452	16.1932 ± 0.0060	138	1.0876 ± 0.0096	57		0	0.00		
	5754	3561	16.2477 ± 0.0014	1777	1.0587 ± 0.0024	745	0.9997 ± 0.0131	33			
	5380	2911	16.3028 ± 0.0016	1618	1.1171 ± 0.0022	743	1.0250 ± 0.0175	32			
	5501	3137	16.3302 ± 0.0019	1318	1.1254 ± 0.0031	389	1.0226 ± 0.0128	33			<i>a</i>
	5719	3523	16.3209 ± 0.0017	1434	1.0906 ± 0.0029	680	1.0328 ± 0.0165	35			
	5430	3014	16.3714 ± 0.0017	1626	1.1235 ± 0.0027	735	1.0223 ± 0.0086	34			
	5746	3556	16.3931 ± 0.0019	1723	1.1230 ± 0.0025	745	1.0665 ± 0.0141	33			<i>a</i>
	6038	4036	16.4230 ± 0.0020	1320	1.1336 ± 0.0028	517	1.0592 ± 0.0099	33			<i>a</i>
	5804	3655	16.5571 ± 0.0020	1626	1.1636 ± 0.0030	457	1.0947 ± 0.0232	31			<i>a</i>
	5500	3139	16.5705 ± 0.0014	2001	1.1799 ± 0.0024	593	1.1063 ± 0.0159	33			
	6043	4048	16.5880 ± 0.0028	1486	1.1862 ± 0.0036	411	1.0765 ± 0.0405	25			
	5363	2877	16.7291 ± 0.0017	1532	1.2342 ± 0.0025	719	1.1475 ± 0.0213	31			
	5710	3508	16.6680 ± 0.0021	1378	1.2011 ± 0.0030	658	1.1197 ± 0.0130	32			
	5839	3704	16.6637 ± 0.0020	2015	1.1962 ± 0.0029	585	1.0950 ± 0.0156	33			<i>a</i>
	5390	2923	16.7092 ± 0.0018	1900	1.2129 ± 0.0025	584	1.1296 ± 0.0134	31			<i>a</i>
	5549	3215	16.8581 ± 0.0204	72	1.2498 ± 0.0239	11		0			<i>b</i>
	5700	3487	16.9410 ± 0.0045	1246	1.2737 ± 0.0052	646	1.1191 ± 0.0256	32			<i>a</i>
	5482	3103	17.0145 ± 0.0018	1843	1.3203 ± 0.0029	568	1.2082 ± 0.0301	34			
	6152	4297	17.1411 ± 0.0036	236	1.3947 ± 0.0069	146		0			
	5355	2857	17.1561 ± 0.0022	1538	1.3598 ± 0.0035	565	1.2381 ± 0.0206	29			<i>a</i>
	5397	2943	17.1754 ± 0.0020	1672	1.4189 ± 0.0034	670	1.2812 ± 0.0176	29			
	6044	4035	17.2250 ± 0.0032	1284	1.3921 ± 0.0043	554	1.2759 ± 0.0234	31			<i>a</i>
	5275	2700	17.2840 ± 0.0036	213	1.4352 ± 0.0046	394	1.2553 ± 0.0433	26			
	5919	3824	17.3165 ± 0.0033	1607	1.4209 ± 0.0055	285	1.2715 ± 0.0424	22			
	6100	4130	17.3778 ± 0.0044	204	1.4360 ± 0.0063	274	1.2827 ± 0.0468	26			
	5561	3262	17.4041 ± 0.0029	101	1.4551 ± 0.0038	678	1.3116 ± 0.0210	24			
	5244	2601	17.4292 ± 0.0038	77	1.4761 ± 0.0102	75	1.3315 ± 0.0460	17			
	5720	3534	17.4359 ± 0.0102	1343	1.4612 ± 0.0138	169		0			
	5891	3801	17.5168 ± 0.0030	1539	1.4632 ± 0.0043	605	1.3240 ± 0.0361	21			
	5399	2948	17.5722 ± 0.0035	193	1.5123 ± 0.0044	536	1.3234 ± 0.0226	24			
	5856	3727	17.6321 ± 0.0032	75	1.5514 ± 0.0045	675	1.4138 ± 0.0401	19			
	5480	3100	17.6454 ± 0.0035	1365	1.5545 ± 0.0049	538	1.3281 ± 0.0358	25			
		3759	17.6587 ± 0.0034	42	1.5293 ± 0.0040	652	1.3741 ± 0.0526	19			
	5875	3774	17.6647 ± 0.0058	353	1.5763 ± 0.0081	642	1.3384 ± 0.0408	18			

Table 5 – *continued*

Sanders	MMJ	Fan	V	N_V	$V - I$	N_I	$B - V$	N_B	P_S	P_G	Notes
	5281	2713	17.7251 ± 0.0065	73	1.5160 ± 0.0075	273		0			<i>b</i>
	5861	3748	17.7940 ± 0.0038	1172	1.5783 ± 0.0044	648	1.3792 ± 0.0556	16			
	5916	3845	17.7913 ± 0.0035	124	1.5797 ± 0.0044	585	1.4139 ± 0.0415	16			
		3636	17.8381 ± 0.0060	396	1.5984 ± 0.0072	631	1.3349 ± 0.0926	13			
Beyond Color Range of Calibration Stars											
	5802	3620	17.95	806	1.60	162		0			
		3322	17.97	59	1.64	625	1.40	14			
	5475	3090	18.00	1027	1.62	625	1.44	14			
	5255	2650	18.04	112	1.66	321	1.44	17			
	5456	3061	18.11	522	1.68	607	1.47	11			
	5957	3891	18.12	187	1.67	583		0			
	5811	3666	18.16	57	1.73	364		0			
	5235	2590	18.33	36	1.75	279		0			
	6115	4181	18.33	405	1.77	229		0			
	6170	4331	18.43	18	1.81	22		0			
	5550	3244	18.48	312	1.79	552		0			
	5231	2589	18.53	320	1.87	270		0			
		4009	18.57	264	1.84	453		0			
	5202	2527	18.57	93	1.83	154		0			
	6207	4402	18.58	36	1.82	80		0			
	5291	2731	18.62	66	1.90	385		0			
	5400	2949	18.63	347	1.80	511		0			
	6150	4276	18.67	178	1.90	160		0			
	5650	3415	18.79	82	1.88	517		0			

Notes: *a*: Star used in the “bluest star” sequence.

b: Star not used in the determining fiducial line.

BSS?: possible blue straggler star

known binary (S1242) that could be mistaken for a normal SGB star in the $(m_{3890}, m_{3890} - m_{9190})$ CMD, but falls among the more numerous and brighter subset of stars in $(m_{6075}, m_{3890} - m_{6075})$ CMD. Since blends *only* fall above the SGB in this portion of either CMD, we select the fainter subset as the likely SSS. The neater appearance of the SGB in $(m_{3890}, m_{3890} - m_{9190})$ is due to the large wavelength separation of the passbands used in the color, which can hide small deviations from the SSS. This should serve as a reminder of the importance of multi-band imaging. The difference between the bright and faint subsets is a few hundredths of a magnitude in m_{6075} .

An implication of this is that the majority of the stars seen near the cluster SGB may be binary stars: S591, S781, S961, S1069, S1239, S1438, and S1487. We have looked at the radial velocities tabulated by Mathieu et al. (1986) for most of our selected stars and these presumed binaries. There were three stars originally in our presumed single group (S1060, S1323, and S2207) and two stars (S961 and S1239) having radial velocity dispersions labelled “hi” ($\sigma \geq 1.0 \text{ km s}^{-1}$) by Girard et al. (1989). However, only S2207 has a large number of measurements and $\sigma > 2 \text{ km s}^{-1}$. We have opted to retain the other two “single” stars in our sample to flesh out the SGB, but this fact should be kept in mind.

At the blue end of the SGB (the local maximum in luminosity of the SSS), it becomes impossible to unambiguously distinguish binaries from single stars based on photometry alone because blends with faint main sequence stars move the system parallel to the SSS. There are a number of stars in this portion of the diagram that could be single stars, so

we resort to simply tabulating all of these and averaging the photometry so that we are not too far off in magnitude.

As for strange stars, Mathieu et al. (2003) have recently discussed the two “sub-subgiant” branch stars S1063 and S1113. Both are known binaries with period of several days, and both are high-probability proper motion members. There is not currently an accepted explanation for the positions of these two stars in the CMD.

3.3.5 The Upper Turnoff

We define this region to be the portion of the SSS between the gap and the local luminosity maximum ($12.65 < V < 12.85$). The number of known binaries falling in this portion of the diagram again indicates that contamination by unresolved blends of stars may be a serious problem. Fig. 10 shows an exploded view of this part of the CMD.

We can get a degree of reassurance from the fact that a number of these systems (specifically S926, S995, S1310, S1589, and S1639) do have multiple radial velocity observations that are consistent both with the cluster mean and with no variation. Once again, we decided to be conservative in our selection in this region, retaining stars and averaging their photometry so that the fiducial could not be far off the SSS. For comparison, we plot corresponding regions of the $(V, V - I)$ CMD for the Montgomery et al. (1993) dataset in Fig. 11. This figure shows the improvement in the photometric scatter near the turnoff, and illustrates the systematic differences stemming from the calibration to the standard system.

Table 6. Unusual Stars in M67

Sanders	MMJ	Fan	V	N_V	$V - I$	N_I	$B - V$	N_B	P_S	P_G	Notes
1054	6489	3347	11.1393 ± 0.0005	2239	1.0706 ± 0.0009	423	1.0810 ± 0.0024	62	0.64	0.99	RGB binary?
1288	6505	4118	11.2502 ± 0.0005	1606	1.0560 ± 0.0014	292	1.0714 ± 0.0015	62	0.96	0.99	RGB binary?
1254	6500	4187	11.4899 ± 0.0005	883	1.0431 ± 0.0007	296	1.0323 ± 0.0037	56	0.95	0.99	RGB binary?
1293	6050	4039	12.1223 ± 0.0004	2163	0.9936 ± 0.0006	636	0.9952 ± 0.0017	62	0.93	0.97	RGB binary?
1001		3075	12.3926 ± 0.0005	1926	0.9874 ± 0.0006	819	0.9659 ± 0.0056	62	0.95	0.99	RGB binary?
489		1770	12.76				0.68		0.95	0.97	TO gap
615	5118	2314	12.818		0.653		0.521		0.96	0.98	TO gap
1271	5969	3904	12.8502 ± 0.0006	1400	0.6148 ± 0.0007	772	0.5238 ± 0.0016	62	0.94	0.99	TO gap
794	5318	2794	12.8650 ± 0.0004	2135	0.9674 ± 0.0009	563	0.9478 ± 0.0048	37	0.93	0.98	RGB binary?
610		2164	12.91				0.49		0.88	0.98	TO gap
1463	6259	4505	12.920 ± 0.015		1.014 ± 0.011		0.983 ± 0.023		0.96	0.98	RGB triple?
602		2026	12.94				0.54		0.93	0.99	TO gap
1503		4705	13.05				0.54		0.87	0.93	TO gap
1575		4970							0.91	0.98	TO gap
2219	5603	3345	13.1829 ± 0.0004	2036	0.6227 ± 0.0006	814	0.5534 ± 0.0033	62	0.99	0.99	BSS?
1292	5961	3889	13.1974 ± 0.0003	2434	0.6936 ± 0.0006	774	0.6178 ± 0.0027	62	0.95	0.98	triple?
816		2829	13.2527 ± 0.0013	411	0.6938 ± 0.0042	26	0.8409 ± 0.0207	13	0.95	0.98	triple?
1220	6125	4214	13.3164 ± 0.0053	354	0.6211 ± 0.0055	272	0.5806 ± 0.0062	51	0.95	0.99	BSS?
773	5377	2904	13.3214 ± 0.0013	1876	0.7120 ± 0.0014	812	0.5826 ± 0.0041	62	0.96	0.99	triple?
1226	6112	4179	13.3357 ± 0.0010	989	0.6336 ± 0.0013	356	0.5499 ± 0.0036	55	0.92	0.98	BSS?
856		2734							0.90	0.87	BSS?
927		3239							0.96	0.98	BSS?
1011	5844	3717	13.8050 ± 0.0006	1996	0.7548 ± 0.0008	811	0.6306 ± 0.0023	61	0.93	0.97	triple?
1608	6443	4956	14.248 ± 0.007		0.833 ± 0.003		0.775 ± 0.011		0.72	0.86	triple?
1249	6144	4258	14.3042 ± 0.0013	663	0.8647 ± 0.0022	274	0.7813 ± 0.0877	30	0.92	0.92	triple?
1492		4654	14.56				0.85		0.85	0.01	triple?
787	5387	2922	14.5636 ± 0.0008	2280	0.9277 ± 0.0011	755	0.8610 ± 0.0035	59	0.05	0.43	member?
1601		5018	14.57				1.02		0.91	0.48	triple?
475		1826							0.92	0.00	triple?
1209	6041	4047	15.6339 ± 0.0020	1611	0.6141 ± 0.0026	359	0.4907 ± 0.0255	28	0.96		??

3.3.6 The Turnoff Gap

Many previous investigators have drawn attention to the gap at the turnoff between $12.85 < V < 13.05$. The gap is the result of short evolutionary time-scales for single stars in this portion of the diagram. We will discuss the phase of single star evolution that is likely to produce this gap in §4.2.2 below. However, we note that there are a number of proper motion members that do fall in this range of magnitudes. There is a possibility that these stars could be single stars, although we believe it is more likely that they should be classified as blue stragglers. Only one cluster member (S1271) fell in the fields we observed, but an examination of the Fan et al. data reveals an additional six (S489, S602, S610, S615, S1503, S1575), none of which has published radial velocity observations.

3.3.7 The Lower Turnoff

For the lower portion of the turnoff region ($13.05 < V < 13.6$), it is once again possible to start to apply a “bluest star” criterion for determining the position of the SSS since the blend sequences no longer intersect the SSS except near the very reddest portion. We still need to be aware of the possibility that some blue stragglers may have to be eliminated. Unfortunately the faint limit of the Mathieu et al. (1986) radial velocity study falls in this range of magnitudes also, so that binaries can now only be eliminated based on photometric variations or on CMD position.

The first apparent feature is formed by four stars (S731, S998, S1230, and S1302) that form a nearly linear feature in all of the CMDs we have examined. All four are high probability cluster members and show no signs of photometric variability (this work; S998, S1230, S1302 in Stassun et al. 2002; S998 in Gilliland et al. 1991), but unfortunately only S998 has been observed spectroscopically. S998 was observed by Melo et al. (2001), who found a radial velocity consistent with the cluster mean, and a low rotational velocity ($v \sin i = 6.3 \pm 0.6 \text{ km s}^{-1}$) consistent with those observed for other turnoff stars. Li has also been detected at the surface of S998 by Hobbs & Pilachowski (1986) at a level consistent with other stars at the turnoff. (To date, there have not been any confirmed detections of lithium in M67 blue stragglers.) While there is no reason to doubt cluster membership and no evidence of variability or of companion stars, the small number of stars involved means that this should be tested further. For example, the bluest star S1230 can be questioned based on its slight fainter m_{6075} magnitude in the Fan et al. CMD. We will discuss these stars more in §4.2.2.

While our color resolution of the turnoff region is somewhat limited, there is clear evidence that stars in this range of magnitudes have evolved to cooler surface temperatures. In this range of magnitudes we begin to tabulate two separate sequences: one based on the bluest reliable cluster member, and one based on weighted averages of groups of stars near the blue edge of the star distribution. In both cases a redward turn is noticeable. Several stars in our VI CMD

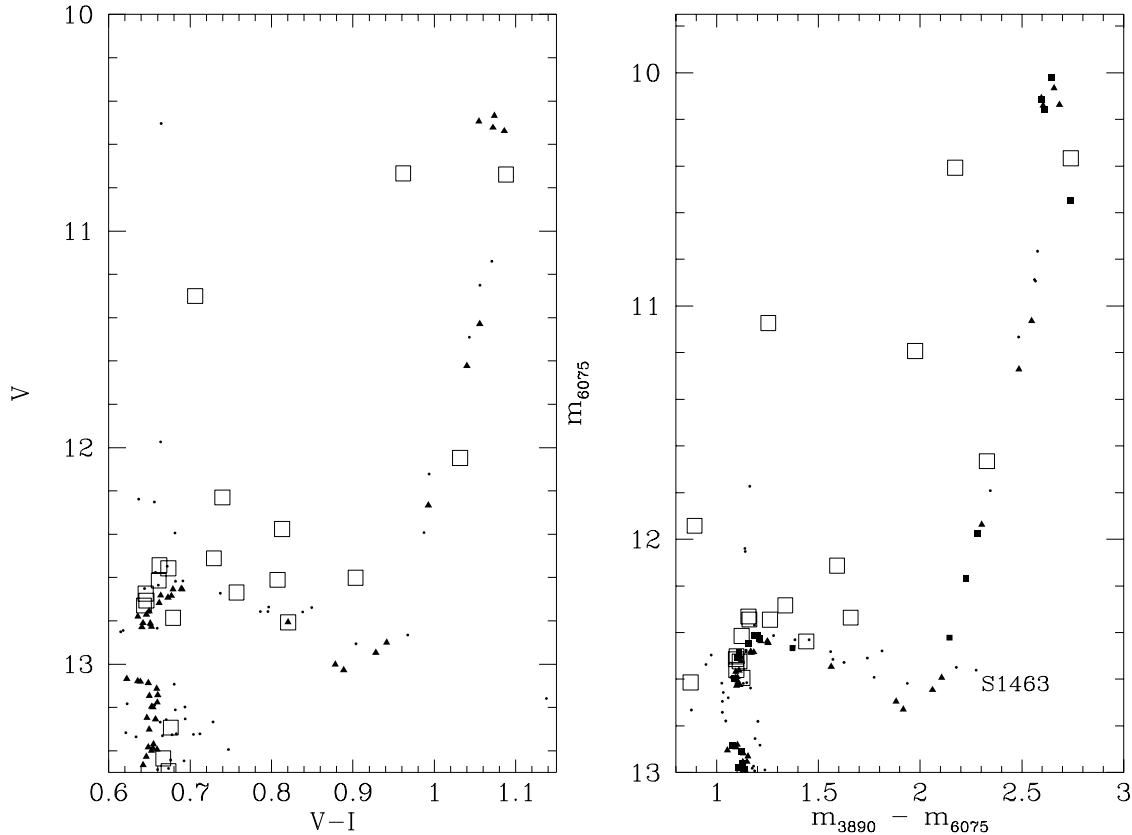


Figure 9. CMDs covering the red giant branch (RGB) and subgiant branch (SGB) from this study (*left panel*) and Fan et al. (1996; *right panel*), including stars selected for the VI fiducial line (*triangles*), additional stars on the fiducial that were not observed in this study (*filled squares*), and known binaries (*open squares*).

can be tentatively classified as blue stragglers based on their CMD positions bluer than the faint portion of the turnoff and fainter than the bright portion of the hook. S856 and S927 were only observed by Fan et al. (1996), but have high membership probabilities. S1220, S1226, and S2219 were observed by us and all have high membership probabilities (see Table 6). However, in the Fan et al. dataset, these stars fall closer to the presumed SSS, although on the blue side of the distribution of colors. The weakest candidate is S1220, which had the largest scatter in measurements and the fewest measurements overall. Other blue stragglers have been discussed elsewhere (e.g., Sandquist & Shetrone 2003b)

Finally, we have looked for cluster members that fall to the red of the two-star blend sequence since stars might be present in this portion of the CMD if they are part of a triple system. We find 4 candidates in our photometry (S773, S816, S1011, and S1292), although these fall within the two-star blend sequence in the Fan et al. ($m_{6075}, m_{3860} - m_{6075}$) CMD. This may be the result of much lower surface temperature for the companion star or stars, since the color in the Fan et al. data more closely resembles $B - V$. We call attention to these stars to encourage further examination.

3.3.8 The Upper Main Sequence

As mentioned in the previous subsection, the SSS for the main sequence can be most cleanly identified using the best measured blue stars at a given magnitude level. We can use proper motion information on the upper main sequence to eliminate potential confusion from the small numbers of field stars that fall very close to the main sequence in the CMD. However, as we have also mentioned, it is apparent that the proper motion membership information becomes less trustworthy for the faintest stars in the samples of Sanders (1977) and Girard et al. (1989).

For $V \gtrsim 15.2$, we allow stars with low proper motion membership probabilities into the sample if they clearly fell near other proper motion members on the main sequence. The faintest star selected for the SSS that has high membership probabilities according to both Sanders (1977) and Girard et al. (1989) is S1291 at $V = 15.29$, so that fainter stars that we retained had low membership probabilities according to either Sanders (1977) or Girard et al. (1989). The faintest star with high probability in just one of the two studies is S769 at $V = 15.61$. At this point the proper motion surveys begin to be seriously incomplete. We do not believe these difficulties bias our measured position for the SSS because the main sequence can be clearly traced throughout.

The star S1209 has a 96% membership probability ac-

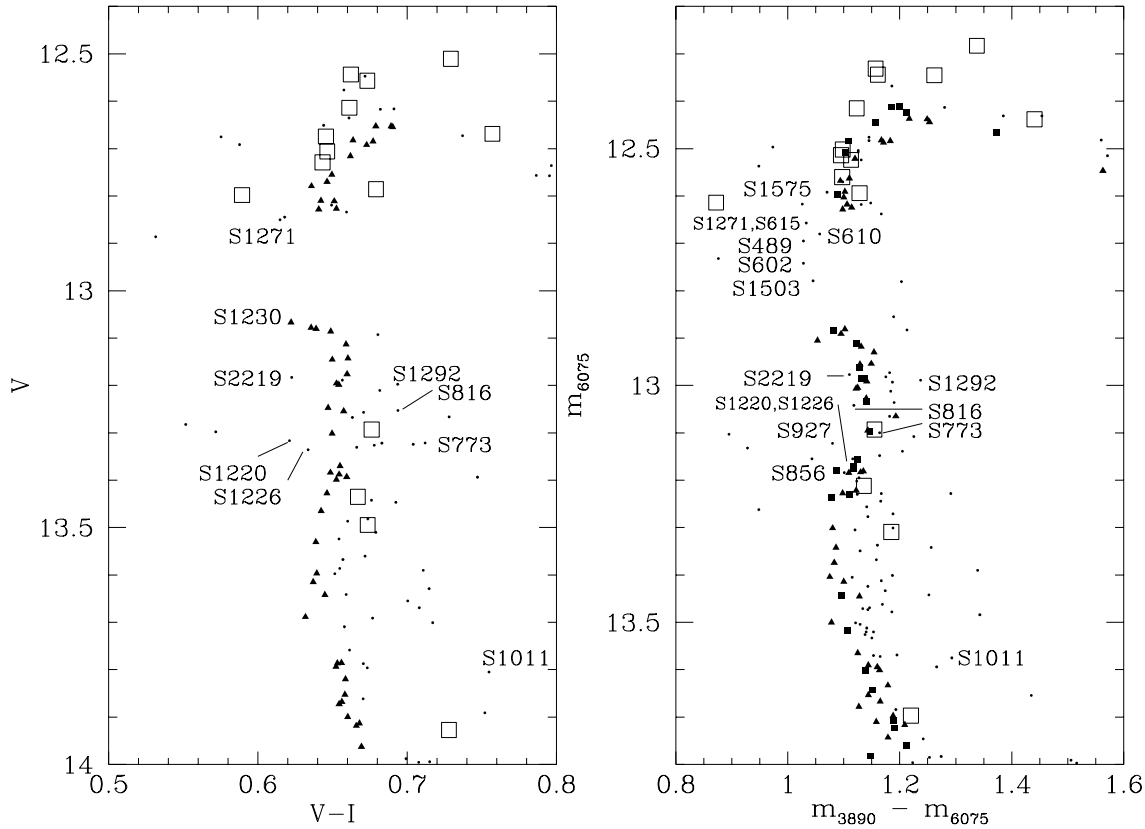


Figure 10. CMDs covering the cluster turnoff. Symbols have the same meaning as in Fig. 9.

cording to Sanders (1977), but is much too blue to be a main sequence star or a blend with a white dwarf star. If this star is indeed a cluster member, we do not have a good explanation for its photometry. We also note that there are several additional stars that fall significantly to the red of the blend sequence in this portion of the color magnitude diagram: S787 and S1249 according to our photometry, and S475, S1492, S1601, and S1608 from Fan et al. (1996). Unfortunately, the proper motion information disagrees on membership for all of these stars except S1249 and S1608. We note that the binary star S1019 (van den Berg et al. 2002) also falls in this portion of the diagram. S1019 is a known X-ray source containing a short-period binary, which makes it possible that another star is present on a much larger orbit. Other systems found to the red of the blend sequence have proper motions that indicate they are nonmembers.

3.3.9 The Lower Main Sequence

For the faintest portions of the main sequence that we studied, CMD position is the only criterion we can use to select stars. Another well-known gap is present on the main sequence at $15.9 \lesssim V \lesssim 16.2$, although there is no obvious explanation for this. As can be seen from Fig. 12, the Fan et al. dataset is no longer useful for selecting stars for the SSS below the gap due to large photometric scatter as the faint limit of the 3890 Å observations is approached at

$m_{3890} \approx 20$. We terminated our tabulation of the fiducial line at $V \approx 17.9$, because the color terms in the photometric transformations cannot be reliably extrapolated beyond the end of the color range of our calibrating stars ($V - I \approx 1.6$). We have, however, tabulated approximate magnitudes and colors for fainter stars that fall on an extension of the main sequence.

4 DISCUSSION

4.1 Distance Modulus

Percival, Salaris, & Kilkenney (2003) have recently published a sample of local G and K dwarfs with accurate Hipparcos parallaxes in a metallicity range appropriate for open cluster main sequence fitting. Percival et al. also describe a method of correcting the dwarf colors for metallicity differences with the cluster that does not require theoretical isochrones. With our new photometric calibration and determination of the cluster's fiducial line, it is worthwhile to attempt to update the distance modulus for the cluster.

In doing the fits to our fiducial points, we eliminated local dwarfs having $(V - I) < 0.83$ from the sample in order to remove any possible effects that stellar evolution might have. [The choice of color cutoff was based on the isochrones of Girardi et al. (2000).] A total of 27 dwarfs with $(V - I) < 1.16$ were used in the fit. We assumed $[\text{Fe}/\text{H}] = 0.02 \pm 0.06$ (Grat-

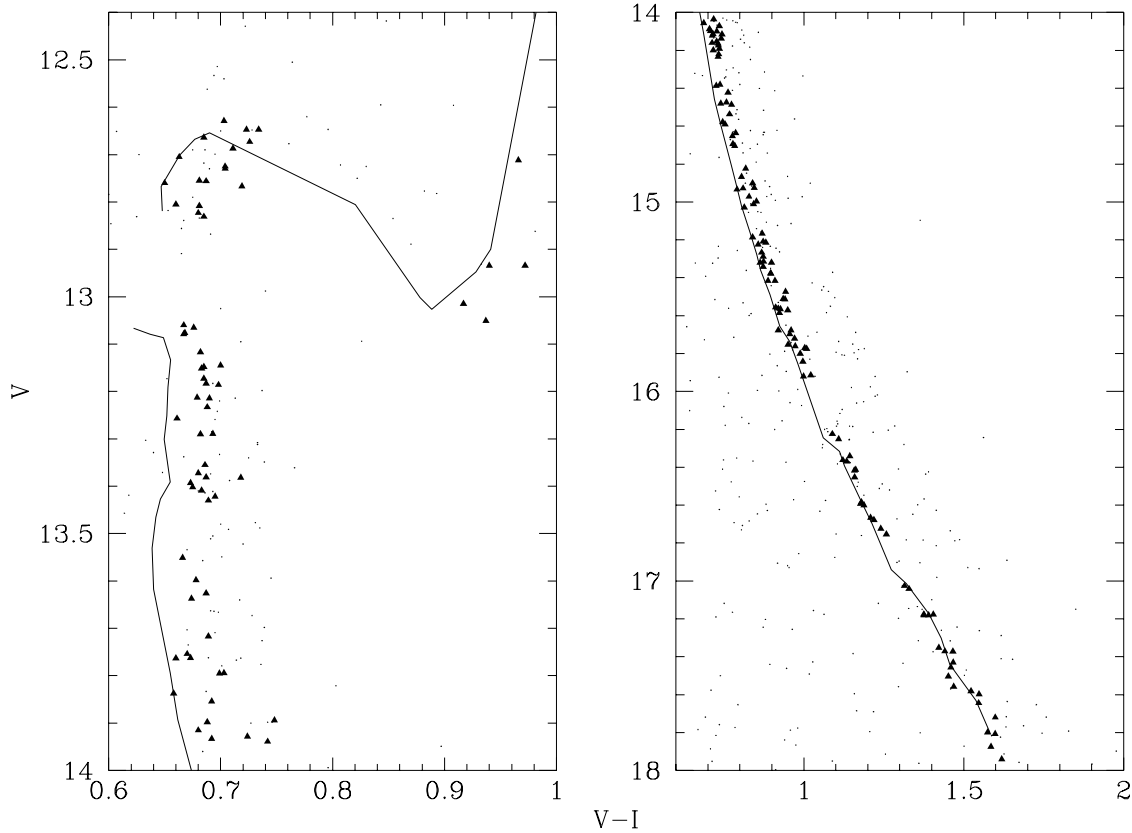


Figure 11. *VI* CMD for M67 using data from Montgomery et al. (1993). The selected single stars from Table 5 are plotted as triangles. The solid lines are fiducial points from this study (Table 4).

ton 2000) and $E(B - V) = 0.04 \pm 0.01$ (corresponding to $E(V - I) = 0.050 \pm 0.013$). We find $(m - M)_0 = 9.60 \pm 0.03$ [$(m - M)_V = 9.72 \pm 0.05$], where the uncertainty includes uncertainty in the fit and in the reddening. The best fit to our fiducial line is shown in Fig. 13. Our derived distance modulus is significantly lower (0.12 mag) than the value given by Montgomery et al. (1993) for an isochrone fit to their *VI* dataset ($(m - M)_V = 9.85$, or $(m - M)_0 = 9.72$), but in good agreement with a recent isochrone fit to the *BV* data of Montgomery et al. (1993) by Sarajedini et al. (1999), giving $(m - M)_V = 9.69 \pm 0.11$. The difference in the distance moduli derived from the *VI* datasets stems from the calibration to the standard system, as can be seen in Fig. 11.

4.2 Comparison with Theoretical Isochrones

A careful comparison between our best measured highest-probability single stars and theoretical isochrones reveals a number of areas of significant disagreement. We focus on recent sets of models by Girardi et al. (2000; hereafter, referred to as Padova isochrones), Yi et al. (2001; hereafter, the Yonsei-Yale or Y^2 isochrones — we use version 2 of these isochrones), and Baraffe et al. (1998; hereafter BCAH).

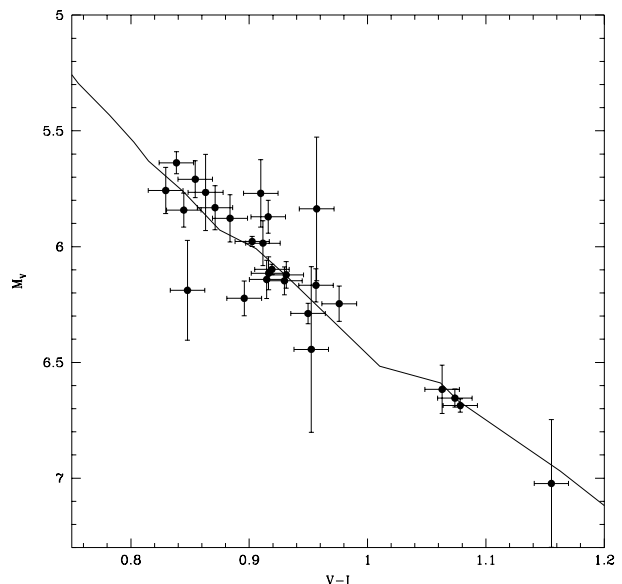


Figure 13. The best fit of our *VI* fiducial line to the metal-rich dwarf star sample of Percival et al. (2003), corresponding to $(m - M)_0 = 9.60$.

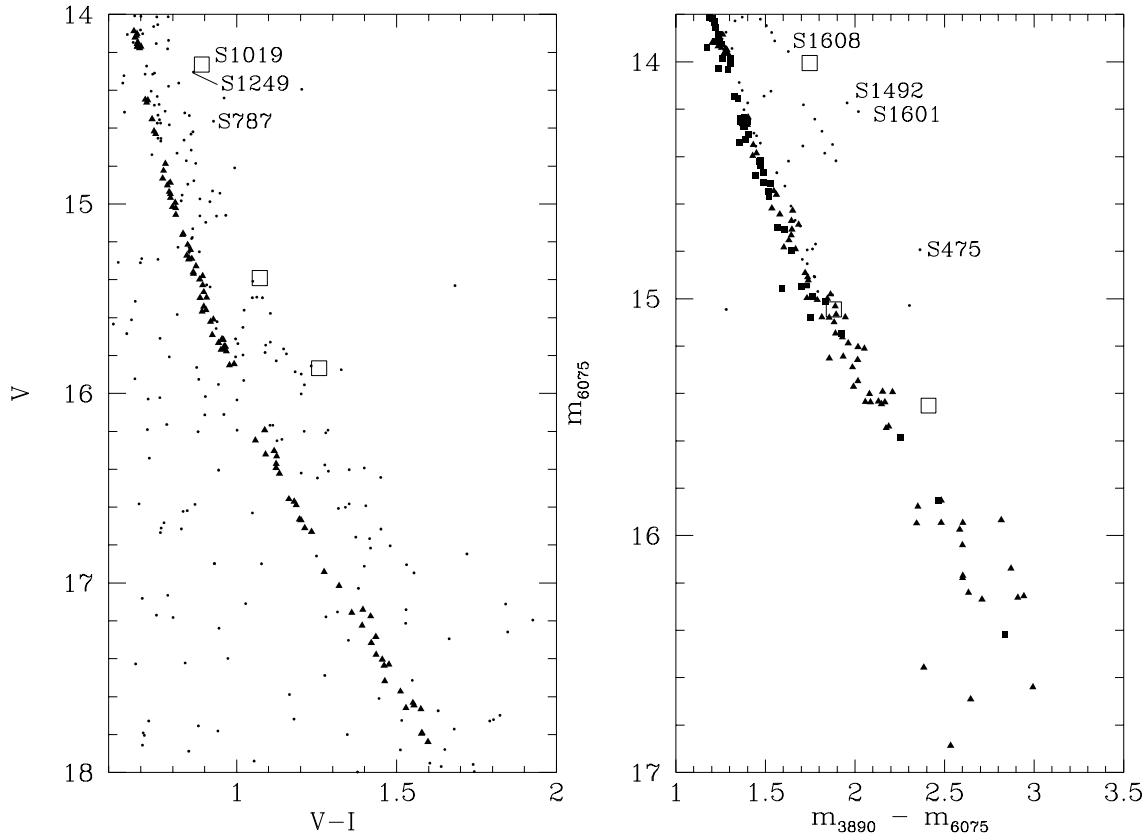


Figure 12. CMDs covering the cluster main sequence. Symbols have the same meaning as in Fig. 9. Dots in the right panel do not represent all of the stars observed by Fan et al. (1996): only those with proper motion information. The faint limit of the m_{3890} data falls within the diagram.

4.2.1 Absolute and Relative Colors of the Upper Main Sequence and Lower Giant Branch

Predicted colors depend critically on the choice of T_{eff} -to-color transformation. The color transformations used in the Padova isochrones are described in Girardi et al. (2002). For most of the area of the CMD we consider, the theoretical colors are based on ATLAS9 synthetic stellar atmospheres (Kurucz 1993) recalculated by Castelli, Gratton, & Kurucz (1997). The Y^2 isochrones employ transformation tables from two different sources: Lejeune, Cuisinier, & Buser (1998; hereafter LCB) and Green, Demarque, & King al. (1987; hereafter GDK). GDK made use of older Kurucz (1979) atmosphere models to predict colors. LCB used empirical solar-abundance color-temperature relations to make corrections to their library spectra (Kurucz 1993) so that the spectra produce color-temperature relations in agreement with empirical solar-abundance relations. Corrected theoretical spectra can then be used to extend the relations to other abundances in a differential sense (Lejeune, Cuisinier, & Buser 1997). Their computed solar-abundance relations generally agree with the empirical ones to better than 0.1 mag. Since M67 is very close to solar abundance, this means that the use of LCB tables should almost be equivalent to using empirical color-temperature relations.

In a direct comparison between the models and obser-

vations, there are differences in the color positions of the unevolved model main sequences. Some error in absolute color is to be expected because the line lists and line parameters used in the theoretical atmosphere models do not accurately reproduce high-resolution spectra (see, for example, the discussion in §3.1.2 of Girardi et al. (2002)), but generally the hope is that these errors average out, particularly when wide bandpasses are used. However, the Padova isochrones are noticeably redder than the Y^2 isochrones with LCB tables at all magnitude levels, in spite of the use of the same set of stellar atmospheres. The smallest color difference occurs near where the solar calibration requires better agreement. Thus, the differences in absolute colors seem to be the result of the *corrections* made to the synthetic photometry.

In the following discussion, we allow for small shifts in color to accommodate the possibility of zero-point errors in the synthetic colors or photometric calibration. The most robust comparison between observations and theory appears to be using a color difference between main sequence stars below the turnoff (where convective overshooting plays a substantial role) and the warmest giants (at the base of the giant branch). If we shift all of the isochrones so that they match M67 stars at the absolute magnitude of the Sun (Fig. 14), we find that only the Y^2 isochrones using the LCB transformation tables roughly reproduce the giant branch

color: the Padova isochrones predict giants that are too red by about 0.03 mag, and the Y^2 isochrones with GDK tables give giants that are too blue by about 0.06 mag. This is not too surprising because of the empirical color-temperature relations used to correct the spectra used to produce the LCB tables. More surprising is the way that the Y^2 -LCB isochrones deviate more strongly from the observed main sequence than the Y^2 -GDK and Padova isochrones. In particular, LCB found that uncorrected theoretical giant spectra deviated more strongly from empirical relations (although mostly higher on the giant branch) than did theoretical dwarf spectra. However, when the GDK tables are used, the theoretical main sequence better matches the observations. In Fig. 2 of Yi et al. (2001) comparing the GDK and LCB color transformations, there is also a feature centered near $\log T_{\text{eff}} = 3.67$ that does not appear in any of the other color transformations. We will discuss this further in §4.2.3 below.

4.2.2 The Shape of the Turnoff

The largest effect on the shape of the turnoff region in M67 is the algorithm used to model convective overshooting in the cores of turnoff-mass stars. Overshooting can be described in terms of the distance (in units of the pressure scale height H_P) a convective element goes beyond the classical boundary defined by the Schwarzschild criterion. In examining the Montgomery et al. (1993) dataset for M67, Dinescu et al. (1995) find that earlier models with overshoot of at most $0.1H_P$ seem to reproduce the observations best although they did not discuss the details of their comparison.

The Padova group isochrones and version 2 of the Y^2 isochrones use similar algorithms to describe the overshooting: no overshooting for low masses ($M < 1.0M_\odot$ for Padova), constant overshoot for higher mass stars ($0.2H_P$ for Y^2 , and approximately $0.25H_P$ for $M \geq 1.5M_\odot$ for Padova). Between these two extremes, the amount of overshoot is ramped linearly. The overshooting parameter in the Girardi et al. models (Λ_c) is described in Bressan, Chiosi, & Bertelli (1991; labelled there as λ), and describes overshooting convective elements moving from *inside* the convective zone, across the classical boundary, and into a radiative region. This is not easily converted to the more typically quoted extent of overshooting beyond the classical edge of the convection zone because it involves the integration of a differential equation for the velocity of a convective element. However, because the acceleration of a convective element becomes negative at the classical convection zone boundary, the overshoot beyond the boundary must be less than one-half the mixing length (Maeder 1975). In the Girardi et al. (2000) models, Λ_c varies as $\Lambda_c = (M/M_\odot) - 1.0$ between 1.0 and $1.5M_\odot$. Stars near the turnoff mass in M67 have $M \approx 1.25M_\odot$, so that the amount of overshoot beyond the zone boundary is less than about $0.13H_P$. Girardi et al. (2000) provide isochrones calculated without convective overshooting, and version 1 of the Y^2 isochrones did not use overshooting for ages similar to that of M67. In Fig. 15, we compare these four sets of isochrones to our observed data for M67. Note that the amount of overshooting given in the figure is for the higher mass range — for stars at the turnoff, the overshooting will be less.

The age of M67 makes it a particularly tricky test of the core convection because M67 is at a stage in which

the morphology of the turnoff star evolutionary tracks changes rapidly as the extent of the convective core decreases with decreasing mass. In addition, the pressure scale height $H_P \rightarrow \infty$ as $r \rightarrow 0$, so that the use of an algorithm forcing overshooting of a constant fraction of H_P is likely to break down in this regime. Roxburgh (1992) and Woo & Demarque (2001) have discussed ways of constraining the amount of overshooting for stars with small convective zones. In the majority of well-studied clusters this is not an important issue, since an age more than a Gyr different than M67’s age is sufficient to make the typical overshoot treatment adequate or to eliminate core convection from cluster stars (e.g. Aparicio et al. 1990). In M67, this issue appears to be critical.

The morphology of the turnoff is the most easily used indicator of the amount of overshooting in the current data. The major changes in morphology from the overshooting are a more noticeable “hook” to the red then blue prior to the SGB, and a change from a more vertical (luminosity change) isochrone to a more horizontal (temperature change) isochrone at the beginning of the SGB (the global T_{eff} maximum). Woo et al. (2003) also discuss the color difference between the turnoff and red giant branch as an indicator of the amount of convective core overshoot. However, based on the results of §4.2.1, current uncertainties in color transformation render this method somewhat questionable at present, particularly because it relies on the *relative* accuracy of dwarf and giant atmosphere models.

The theoretical interpretation of the features is that the reddest extent of the “hook” corresponds to the beginning of a rapid phase of shrinkage of the extent of convection in the core of the star. At the same time the core hydrogen content is quickly approaching exhaustion, which occurs at the bluest point on the isochrone. Following this, a hydrogen fusion shell source is established around the core. Overshooting significantly affects evolutionary time-scales, most notably lengthening the star’s main sequence life. It also affects the length of the beginning of the subgiant phase by allowing more of the hydrogen *near* the centre to be consumed, which requires a more substantial and rapid adjustment of structure when the core hydrogen is exhausted. Thus, the distribution of stars in the vicinity of the turnoff on a CMD carries information about the amount of overshooting, although this can be difficult to extract in the case of a relatively star-poor cluster like M67.

There are other difficulties in interpreting M67’s CMD, however. In terms of the observational morphology of the turnoff, we are faced with a “hook” that appears to require some overshooting, but with an extent less than seen in either of the theoretical isochrones with overshooting. The redward-pointing portion of the hook is well-populated and clearly at odds with all of the theoretical isochrones without overshooting. If the four stars we identified in §3.3.7 are truly single stars that are part of the blueward-pointing portion of the “hook”, this also can only be explained with small amounts of overshooting. For example, fig. 5 of Woo et al. (2003) presents synthetic CMDs incorporating different amounts of overshooting for a somewhat younger cluster. Only the models with overshooting of $0.1H_P$ have a significant number of single stars on the red half of the blueward-pointing part of the hook and on the bluest parts of the SGB. In addition, higher amounts of overshooting cause the red

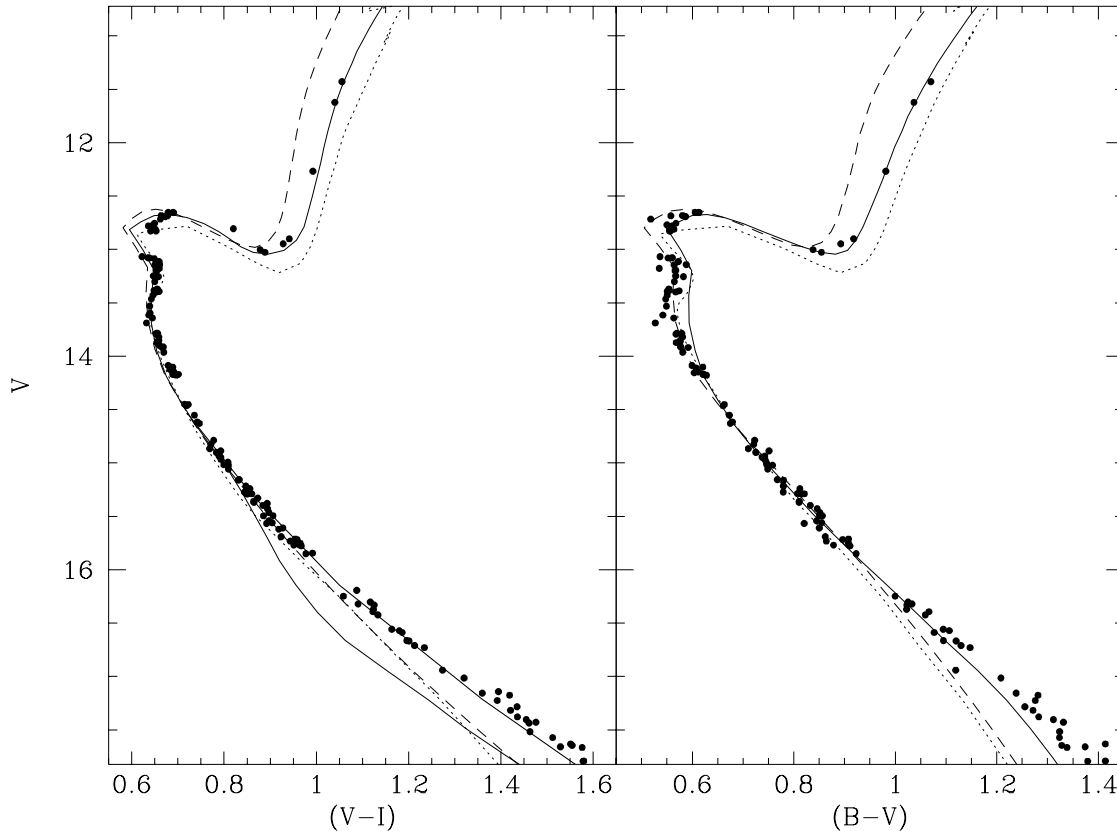


Figure 14. A comparison of our selected M67 stars (*solid points*) with theoretical isochrones for 4 Gyr from the Yale-Yonsei group (*solid line*: Lejeune et al. 1998 color transformations; *dashed line*: Green et al. (1987) transformations), Padova group (*dotted line*: Girardi et al. 2000), and Baraffe et al. (1998; *heavy solid line*). The isochrones have been shifted using $(m - M)_V = 9.72$, with an additional color shift (to account for reddening and zero-point offsets in the color- T_{eff} relations) to match the data at $V \approx 14.5$. The color shifts were 0.03 in $V - I$ and 0.04 and 0.025 for the two Yale-Yonsei isochrones, 0.0 and 0.005 for Padova, and 0.01 for Baraffe et al. (no $B - V$ models).

portion of the hook to overlap the cluster’s blend sequence, something which is not seen in M67. However, the bluest portion of the subgiant branch appears to most closely resemble the no-overshoot models, particularly those of the Padova group.

The manner of our star selection makes it impractical to do a detailed analysis of the numbers of stars in the CMD to examine issues of evolutionary time-scales. However, the mere presence of the gap is interesting. Typically turnoff gaps seen in clusters like M67 have been associated with the shrinkage of the convective core prior to hydrogen exhaustion. However, models indicate that one of the most noticeable differences when overshooting is introduced is the drastic decrease in the amount of time spent on the bluest parts of the SGB immediately after hydrogen exhaustion (see Fig. 16). If the four stars are indeed on the blueward-pointing portion of the hook, they give the impression that the evolutionary tracks should evolve more in luminosity than in surface temperature at the beginning of the SGB, and that the models should be evolving more quickly at the beginning of the SGB to explain the gap. This is crudely consistent with presence of some overshooting, although the exact morphology of the isochrone is still puzzling. Helium

diffusion could play an interesting role for M67 turnoff stars by helping to bring additional hydrogen fuel toward the core. The models of the Padova group do not include helium diffusion, while those of the Y^2 group do.

Our best interpretation of the turnoff morphology is that a fairly small convective core including some amount of convective overshoot is necessary, but that the extent of the mixed core at hydrogen is small. Because the evolutionary time-scale for the stars increases dramatically once the hydrogen fusion regions reach hydrogen rich gas outside of the regions earlier occupied by a convective core, the presence of a gap puts a lower limit on the extent of the core. If the convective core in a turnoff star is never particularly large, then after core hydrogen exhaustion the situation is similar to that of a lower mass star. If there is not a large region of hydrogen-exhausted gas near the core, then the star does not need to adjust its structure much to find a new, stable configuration. In this sense, the gap in an old cluster like M67 can be said to be the last remnant of the Hertzsprung gap seen in much younger open clusters: when core hydrogen is exhausted in turnoff stars in those clusters, a greater degree of structural readjustment is necessary.

Our interpretation of these features does depend on a

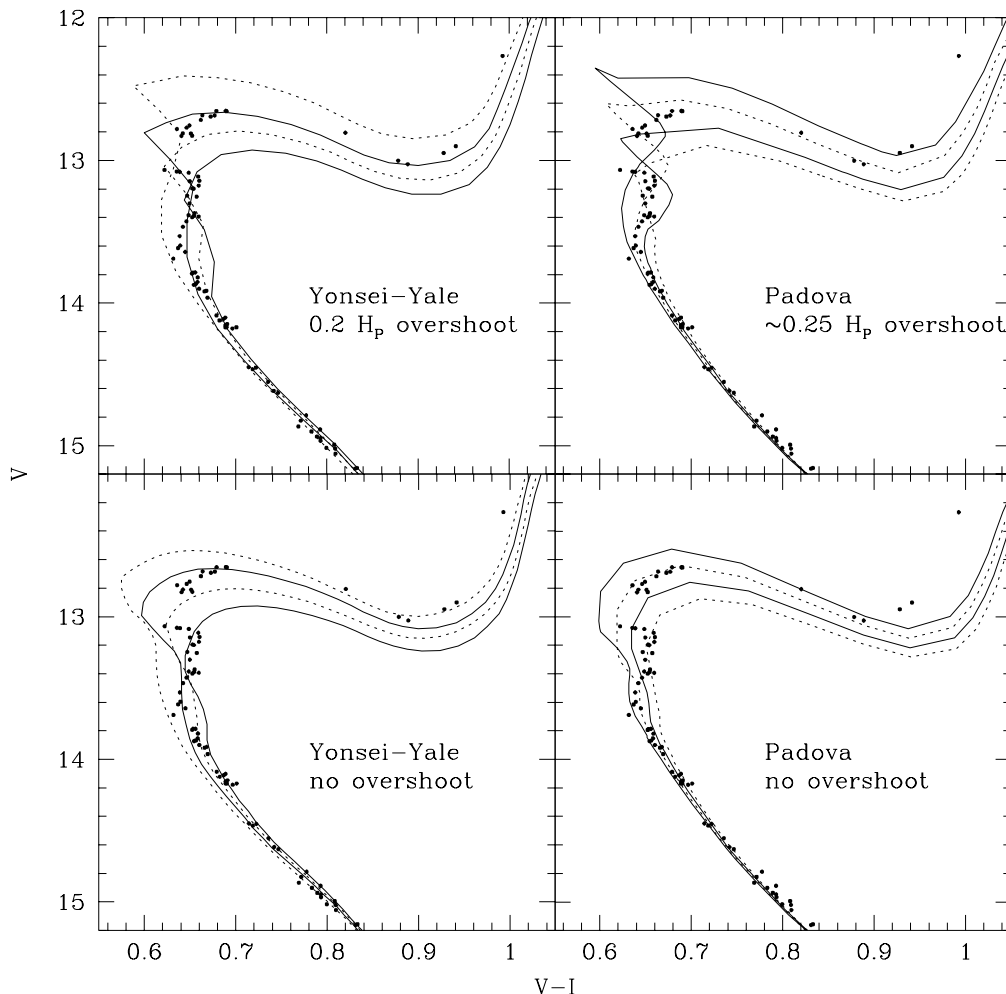


Figure 15. Comparisons between our M67 observations and isochrones from the Yonsei-Yale and Padova groups with and without convective core overshooting. From brightest to faintest on the subgiant branch, the isochrones are for ages 3.5, 4, 4.5 and 5 Gyr.

small number of stars, some of which could be blue stragglers or unresolved binaries. If all or most of them are single stars though (as we believe), the morphology of the turnoff deserves a more detailed look because it can tightly constrain the behavior of gas in small convective cores.

The exact amount of overshoot has only a small effect on the age inferred from M67’s turnoff. However, 4 Gyr isochrones reproduce most aspects of the upper main sequence and subgiant branch well, so we regard this as the preferred age, and estimate that the uncertainty is less than about 0.5 Gyr. This is in agreement with the value derived by Dinescu et al. (1995), although they used an earlier set of models and different photometry.

4.2.3 The Shape of the Main Sequence

Using $V-I$ color, the Y²-GDK and Padova isochrones agree with each other and satisfactorily match the shape of the main sequence nearly to $V = 16$. The Y²-LCB isochrone diverges rather substantially from the M67 SSS by $V = 15.5$.

In all three cases though, the main sequence models become far too blue. We find that the solar-metallicity models of BCAH provide a much better fit to the shape of the main sequence down to the limit of our calibration at $V = 17.8$. In $B-V$ color, the Padova and Y²-GDK isochrones still agree, but the Y²-LCB isochrones is a much closer fit to the actual data to $V \approx 16.75$ (see Fig. 14). This is a clear indication that the color- T_{eff} relations are responsible for much of the disagreement when it comes to fitting the main sequence.

One of the reasons the main sequence color calibration is so difficult is the lack of a good, independently-determined T_{eff} scale for faint dwarfs. Houdashelt, Bell, & Sweigart (2000) examined data for cool ($4000 \text{ K} \leq T_{\text{eff}} \leq 6500 \text{ K}$) field stars and found indications that the color- T_{eff} relations for dwarfs and giants diverge for $T_{\text{eff}} < 5000 \text{ K}$ in $(V-R)_C$ and $(V-I)_C$ colors. According to their data, the dwarf stars become redder than the giants at a given T_{eff} , which is in the correct direction to explain the discrepancies between models and observations of M67. This could be the result of gravity-sensitive molecular features like TiO and CN that

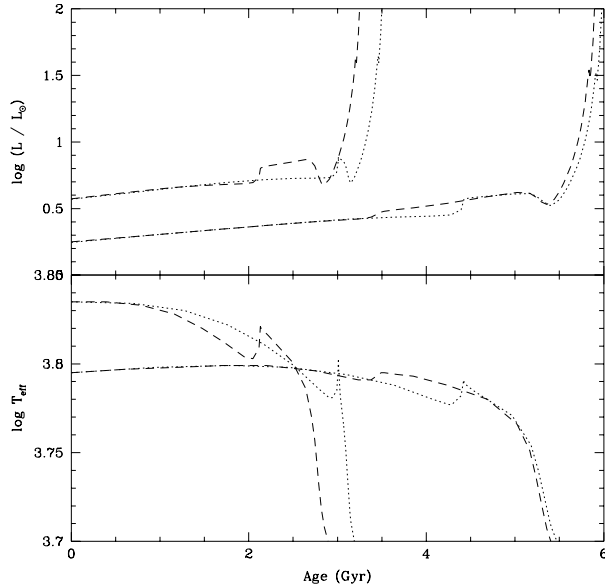


Figure 16. The runs of $\log(L/L_{\odot})$ and $\log T_{\text{eff}}$ versus age for $1.2M_{\odot}$ (heavy lines) and $1.4M_{\odot}$ (thin lines) evolutionary tracks from the Padova group with (dotted lines) and without (dashed lines) convective core overshooting.

fall in V , R , and I bands (Houdashelt et al. 2000). The empirical color- T_{eff} relations used to correct the models of LCB (Bessell 1979, 1995) are systematically bluer than the Houdashelt et al. field dwarf values (see their fig. 12), and Bessell (1979) actually used field giant data to set the relation for cool dwarfs, assuming the two are equivalent. But as Houdashelt et al. state, systematic errors in T_{eff} measurements for the coolest dwarfs could also be responsible for the differences between field dwarf and field giant color- T_{eff} relations.

According to empirical relations, $T_{\text{eff}} = 5000\text{K}$ corresponds to $(V - I)_0 = 0.93$. In our M67 data, this roughly corresponds to the color at which the Padova and Y^2 -GDK isochrones begin diverging from the bluest stars on the M67 main sequence. The Y^2 -LCB models diverge closer to $(V - I) = 0.85$, which appears to be due to a lack of empirical data to calibrate the $(V - I) - T_{\text{eff}}$ relation (P. Westera, private communication).

The primary differences in input physics between the best-fitting models of BCAH and those of the Y^2 and Padova groups are in the equation of state and in the surface boundary conditions. BCAH use recent non-grey stellar atmosphere models as boundary conditions for their stellar models and the equation of state of Saumon, Chabrier, & Van Horn (1995; hereafter SCVH). The Padova isochrones make use of the MHD equation of state (Mihalas et al. 1990) and opacities from Alexander & Ferguson (1994) for surface layers. The Y^2 isochrones also use Alexander & Ferguson (1994) opacities at the stellar surface. For the equation of state they use the OPAL (Rogers et al. 1996) tables at temperatures down to $\log T = 3.7$, and then revert to a Saha equation of state with Debye-Hückel correction for Coulomb interactions.

SCVH have shown that significant differences exist be-

tween their equation of state and others, and that the MHD or OPAL equations of state are the most accurate for stars of solar mass or above while the SCVH equation of state is preferred for low mass stars due to its inclusion of non-ideal effects and molecule formation. However, Chabrier & Baraffe (1997) indicate that comparisons of models calculated using the SCVH and MHD equations of state show agreement to better than 1.3% in T_{eff} and L for stars with $M \gtrsim 0.4M_{\odot}$. The Y^2 models used a simpler equation of state at low temperatures ($\log T < 3.7$). The Y^2 models reach this threshold in the surface layers for stars with mass near $0.81M_{\odot}$ ($M_V \approx 6.3$), which appears to be at a point on the main sequence that is too faint to explain the deviations. So, our feeling is that current equation of state differences are not likely to be of high importance in the range of star masses we have observed.

At low T_{eff} , studies (e.g. Chabrier & Baraffe 1997) have forcefully shown the importance of the surface boundary condition in determining the luminosity and spectral type of the star. For fully convective stars, the temperature gradient is forced to be very close to the adiabatic temperature gradient, so that the surface conditions (where the adiabaticity breaks down) essentially set the entire interior structure of the star. Unfortunately, stellar atmospheres at low T_{eff} are strongly non-grey (e.g. Chabrier & Baraffe 1997), so that to adequately determine the interior structure, detailed stellar atmospheres have to be used as surface boundary conditions. While the BCAH models diverge from deep photometry of open clusters for $T_{\text{eff}} < 3700\text{K}$ (Chabrier & Baraffe 1997), this limit is fainter on the main sequence than either the Padova or Y^2 have been tested. In addition, BCAH use color transformation tables derived in a self-consistent way from their model atmospheres while the Padova and Y^2 isochrones use tables derived from atmospheres that are not applied as surface boundary conditions. These are the primary reasons behind the different CMD positions of the BCAH main sequence and those of the Padova and Y^2 groups.

Differences between the isochrones due to the assumed equation of state, color-temperature transformations, and surface boundary conditions get severe the fainter on the main sequence the models go (e.g. von Hippel et al. 2002). As yet, the Y^2 and Padova isochrones have not been rigorously tested in this regime (see Yi et al. 2001), so it is not entirely fair to expect agreement as yet. However, when the models are shifted to match up with the observed data at the magnitude level of the Sun (thereby differentially removing small effects of the differences in age and composition, and the larger effects of differences in color zero points) all of the models except those of BCAH are clearly too blue. von Hippel et al. (2002) found a similar discrepancy extending to fainter levels for the cluster M35. However, M67 has a composition that is closer to that of the Sun, and so *should* closely match the solar neighborhood stars used to calibrate color- T_{eff} relations.

5 CONCLUSIONS

We have used the extensive database of observations we have gathered in our variability studies to produce a high-precision CMD for the old solar-abundance open cluster

M67. The age of M67 has created turnoff stars that are showing the effects of overshooting in their small convective cores. M67 thereby provides a severe test of algorithms used to model stars with masses $1.1 \lesssim M/M_{\odot} \lesssim 1.3$.

If M67 data is calibrated to fainter magnitudes in the future, it will be possible to more strongly test the physics involved in the computation of the stellar atmospheres of main sequence dwarfs. Because of the solar abundance of the cluster, M67 can be extremely valuable in constraining color transformations for main sequence stars of solar abundance. Because solar abundance stars often provide the basis for determining the transformations at lower abundances, the data for M67 has wide application.

The accurate determination of the lower main sequence fiducial line would also open the possibility of predicting the properties of both stars in unresolved binaries having mass ratios with $q \lesssim 0.7$. In this range, a binary system can be uniquely deconvolved into its components under the assumption that there are just two non-interacting stars. Our photometry does not go deep enough down the main sequence to allow us to make this deconvolution without additional data. With just the addition of a reasonably good theoretical main sequence line, it would be possible to determine a photometric mass ratio distribution for a fairly large sample of stars in this cluster. Because M67 appears to be a cluster that is quite relaxed dynamically, this would give us the opportunity of directly seeing how the cluster dynamics have affected the binary stars.

ACKNOWLEDGMENTS

E.L.S. would like to thank the director of Mount Laguna Observatory (P. Etzel) for generous allocations of telescope time that made this study possible, M. Shetrone for many useful conversations, M. van den Berg for very useful conversations and for thorough comments on the manuscript, P. Westera for insight into T_{eff} -color relations, and the anonymous referee for valuable comments about mechanisms broadening a single star sequence that resulted in §3.2. This research has made use of the SIMBAD database operated at CDS, Strasbourg, France, and was supported in part by the National Science Foundation under Grant No. AST-0098696.

REFERENCES

- Alexander D. R., Ferguson J. W., 1994, *ApJ*, 437, 879
Aparicio A., Bertelli G., Chiosi C., Garcia-Pelayo J. M. 1990, *A&A*, 240, 262
Balachandran S., 1995, *ApJ*, 446, 203
Baume G., Vázquez R. A., Feinstein A., 1999, *A&A*, 137, 233
Baraffe I., Chabrier G., Allard F., Hauschildt P., 1998, *A&A*, 337, 403 (BCAH)
Bergeron P., Wesemael F., Beauchamp A., 1995, *PASP*, 107, 1047
Belikov A. N., Kharchenko N. V., Piskunov A. E., Schilbach E., 2000, *A&A*, 358, 886
Belloni T., Verbunt F., Mathieu R. D., 1998, *A&A*, 339, 431
Bessell M. S., 1979, *PASP*, 91, 589
Bessell M. S., 1995, in Tinney C., ed., *ESO Workshop, The Bottom of the Main Sequence and Beyond*. Springer-Verlag, Berlin, p. 123
Bressan A. G., Chiosi C., Bertelli G., 1981, *A&A*, 102, 25
Brown J. A., 1987, *ApJ*, 317, 701
Castelli F., Gratton R., Kurucz R. L., 1997, *A&A*, 318, 841
Chabrier G., Baraffe I., 1997, *A&A*, 327, 1039
Chevalier C., Ilovaisky S. A., 1991, *A&AS*, 90, 225
Dinescu D. I., Demarque P., Guenther D. B., Pinsonneault M. H., 1995, *AJ*, 109, 2090
Fan, X. et al., 1996, *AJ*, 112, 628
Gilliland R. L. et al., 1991, *AJ*, 101, 541
Gilroy K. K., Brown J. A., 1991, *ApJ*, 371, 578
Girard T. M., Grundy W. M., Lopez C. E., Van Altena W. F., 1989, *AJ*, 98, 227
Girardi L., Bressan A., Bertelli G., Chiosi C., 2000, *A&AS*, 141, 371 (Padova)
Girardi L., Bertelli G., Bressan A., Chiosi C., Groenewegen M. A. T., Marigo P., Salasnich B., Weiss A., 2002, *A&A*, 391, 195
Gratton R., 2000, in Pallavicini R., Micaela G., Sciortino S., eds, *ASP Conf. Ser. Vol. 198, Stellar Clusters and Associations: Convection, Rotation, and Dynamos*. Astron. Soc. Pac., San Francisco, p. 225
Green E. M., Demarque P., King C. R., 1987, *The Revised Yale Isochrones and Luminosity Functions*. Yale Univ. Obs., New Haven, CN
Hobbs L. M., Pilachowski C., 1986, *ApJ*, 311, L37
Houdashelt M. L., Bell R. A., Sweigart A. V., 2000, *AJ*, 119, 1448
Honeycutt R. K., 1992, *PASP*, 104, 435
Janes K. A., Smith G. H., 1984, *AJ*, 89, 487
Joner M. D., Taylor B. J., 1990, *PASP*, 102, 1004
Jones B. F., Fischer D., Soderblom D. R., 1999, *AJ*, 117, 330
Kurucz R. L., 1979, *ApJS*, 40, 1
Kurucz R. L., 1993, in Barbuy B., Renzini A., eds, *IAU Symp. 149, The Stellar Populations of Galaxies*. Kluwer, Dordrecht, p. 225
Landolt A. U., 1992, *AJ*, 104, 340
Lejeune Th., Cuisinier F., Buser R., 1997, *A&A*, 125, 229
Lejeune Th., Cuisinier F., Buser R., 1998, *A&A*, 130, 65
Maeder A., 1975, *A&A*, 40, 303
Mathieu R. D., Latham D. W., Griffin R. F., Gunn J. E., 1986, *AJ*, 92, 1100
Mathieu R. D., Latham D. W., Griffin R. F., 1990, *AJ*, 100, 1859
Mathieu R. D., van den Berg M., Torres G., Latham D., Verbunt F., Stassun K., 2003, *AJ*, 125, 246
Melo C. H. F., Pasquini L., De Medeiros J. R., 2001, *A&A*, 375, 851
Mihalas D., Hummer D. G., Mihalas B. W., Däppen W., 1990, *ApJ*, 350, 300
Montgomery K. A., Marschall L. A., Janes K. A., 1993, *AJ*, 106, 181
Percival S. M., Salaris M., Kilkenny D., 2003, *A&A*, 400, 541
Richer H. B., Fahlman G. G., Rosvick J., Ibata R., 1998, *ApJ*, 504, L91
Rogers F. J., Swenson F. J., Iglesias C. A., 1996, *ApJ*, 456, 902 (OPAL)

- Roxburgh I. W., 1992, *A&A*, 266, 291
Rucinski S. M., Duerbeck H. W., 1997, *PASP*, 109, 1340
Sanders W. L., 1977, *A&AS*, 27, 89
Sandquist E. L., Latham D. W., Shetrone M. D., Milone A. A. E., 2003a, *AJ*, 125, 810
Sandquist E. L., Shetrone M. D., 2003b, *AJ*, 125, 2173
Sandquist E. L., Shetrone M. D., 2003c, *AJ*, submitted
Sarajedini A., von Hippel T., Kozhurina-Platais V., Demarque P., 1999, *AJ*, 118, 2894
Shetrone M. D., Sandquist E. L., 2000, *AJ*, 120, 1913
Saumon D., Chabrier G., Van Horn H. M., 1995, *ApJS*, 99, 713 (SCVH)
Soderblom D. R., King J. R., Siess L., Jones B., Fischer D., 1999, *AJ*, 118, 1301
Stassun K. G., van den Berg M., Mathieu R. D., Verbunt F., 2002, *A&A*, 382, 899
Stetson P. B., 1987, *PASP*, 99, 191
Stetson P. B., 1990, *PASP*, 102, 932
Stetson P. B., 1992, *JRASC*, 86, 71
Stetson P. B., 2000, *PASP*, 112, 925
van den Berg M., Orosz J., Verbunt F., Stassun K., 2001, *A&A*, 375, 375
van den Berg M., Stassun K. G., Mathieu R. D., Verbunt F., 2002, *A&A*, 382, 888
von Hippel T., Steihauser A., Sarajedini, A., Deliyannis C. P., 2002, *AJ*, 124, 1555
Wilden B. S., Jones B. F., Lin D. N. C., Soderblom D. R., 2002, *AJ*, 124, 2799
Woo J.-H., Demarque P., 2001, *AJ*, 122, 1602
Woo J.-H., Gallart C., Demarque P., Yi S., Zoccali M., 2003, *AJ*, 125, 754
Yi S., Demarque P., Kim Y.-C., Lee Y.-W., Ree C. H., Lejeune T., Barnes S., 2001, *ApJS*, 136, 417 (Y^2)
Zhao J. L., Tian K. P., Pan R. S., He Y. P., Shi H. M., 1993, *A&AS*, 100, 243